ISSN: 2667-8977
E-ISSN: 2687-3834

VOLUME 3 - ISSUE 2
DECEMBER 2021

JOURNAL OF MEDICAL INNOVATION AND TECHNOLOGY

Eskisehir Osmangazi University Publications

WWW.JOMIT.ORG

Cilt: 3 Sayı: 2 Aralık 2021

Yayın Periyodu / Publication Period : Yılda 2 kez yayınlanır.
Haziran – Aralık

Yazışma Adresi / Correspondence Address: Osmangazi Üniversitesi Tıp Fakültesi Dekanlığı
Meşelik Yerleşkesi 26480 Eskiehir/ Türkiye
Tel: 0222 2392979 - 4489 Fax: 0222 2393772
e-mail: info@jomit.org
e-mail: otd@ogu.edu.tr
web : http://jomit.org
https://dergipark.org.tr/tr/pub/jomit

Baskı / Printed by : ESOGÜ Basım Evi
Tel: 0222 2393750 – 3105
e-mail: esogugrafik@gmail.com

MEDİKAL İNOVASYON VE TEKNOLOJİ DERGİSİ

Journal of Medical Innovation and Technology

YAZARLARI BİLGİLENDİRME

Medikal İnovasyon ve Teknoloji Dergisi, Eskişehir Osmangazi Üniversitesi Tıp Fakültesi'nin resmi yayın organıdır. Klinik ve deneysel çalışmalar, olgu sunumları, derlemeler, editöre mektup ve tıp alanında klinik haber olmak üzere hakemli ve açık erişimli bir dergidir. Dergi Haziran ve Aralık aylarında olmak üzere yılda iki kez çıkarılır. Derginin dili Türkçe/İngilizce dir. Yazıların dergide yer alabilmesi için daha önce başka bir dergide yayınlanmamış olması ve yayınlanmak üzere gönderilmemiş olması gerekmektedir.

A4 boyutunda, çift aralıklı, 12 punto ile, sayfanın tüm kenarlarında en az 2.5 cm boşluk kalacak şekilde yazılmalı ve toplam 16 sayfayı aşmamalıdır. Yazının içerisinde mutlaka bir başlıklandırma yapılmalıdır. Ana başlıklar numara verilmeden, koyu ve büyük harfle yazılmalıdır. Tüm başlıklar paragrafın ilk satırı ile aynı hizada olmalıdır. Yazılarda System International (SI) birimleri kullanılmalıdır. Başlıklar derecesine göre aşağıda gösterilen şekilde olmalıdır:

- MAKALE BAŞLIĞI (Cambria, 12 Punto, Koyu)
- ÖZ (Cambria, 9 Punto, Koyu)
- ABSTRACT (Cambria, 9 Punto, Koyu)
- GİRİŞ (Cambria, 10 Punto, Koyu)
- Birinci Ana Başlığın Alt Başlığı (Cambria,10 Punto, Koyu)
- Birinci ana başlığın alt başlığının alt başlığı (Cambria,10 Punto, Koyu değil)
- GEREÇ ve YÖNTEM (Cambria,10 Punto, Koyu)
- BULGULAR (Cambria, 10 Punto, Koyu)
- TEŞEKKÜR (Cambria, 10 Punto, Koyu)
- KAYNAKÇA (Cambria, 10 Punto, Koyu)

Dipnot açıklamaları Cambria 9 punto, Tablolar ve Şekiller ise Cambria 9 punto, tek satır aralıklı olarak düzenlenmelidir. Şekil adları şeklin altında, tablo adları tablonun üstünde yer almalı; şayet alıntı yapılmışsa kaynak şekil ve tablonun altında gösterilmelidir. Tablolarda satır ve sütün çizgileri kullanılmamalıdır.

Tablo, şekiller ve resimler ayrı dosyalarda iletilmelidir. Şekiller ve resimler JPEG formatında en az 300dpi olmalıdır.

Metin içindeki tüm şekil ve tablolara atıfta bulunulmalıdır. Tablo ve Şekiller (Çizim ve Fotoğraflar) cümle sonunda parantez içinde rakam ile (1, 2, 3) şeklinde belirtilmelidir. Şekillerin ve tabloların alt yazıları ayrı bir sayfaya yazılmalıdır.

Araştırma yazıları ve Kısa bildiriler aşağıdaki sıraya göre hazırlanmalıdır

- Başlık sayfası
- Öz (özet) (Amaç, Gereç ve Yöntem, Bulgular, Sonuç olarak kısımlara ayrılmalıdır.)
- Abstract (Objective, Materials and Methods, Results, Conclution)
- Giriş
- Gereç ve Yöntem
- Bulgular
- Tartışma
- Teşekkür
- Kaynaklar

Araştırma yazıları

Öz ve Abstract 150-400 kelime olmalıdır.

Metnin tamamı (Türkçe ve İngilizce özetler dahil, kaynaklar hariç) 5000 kelimeyi aşmamalıdır.

Gereç ve Yöntem kısmında Etik Kurul Onayı şeklinde alt başlık bulunmalı ve burada onayın alındığı kurulun ismi belirtilmelidir.

Araştırmaya finansman/katkı sağlayan kuruluş ya da kişilere yapılacak teşekkür tartışma ile kaynaklar arasında yer almalıdır.

Kaynaklar en fazla 50 adet olmalıdır.

Kısa bildiriler

- Öz ve Abstract 150-400 kelime olmalıdır.
- Metnin tamamı (Türkçe ve İngilizce özetler dahil, kaynaklar hariç) 2000 kelimeyi aşmamalıdır.
- Gereç ve Yöntem kısmında Etik Kurul Onayı şeklinde alt başlık bulunmalı ve burada onayın alındığı kurulun ismi belirtilmelidir.
- Araştırmaya finansman/katkı sağlayan kuruluş ya da kişilere yapılacak teşekkür tartışma ile kaynaklar arasında yer almalıdır.
- Kaynaklar en fazla 25 adet olmalıdır.

Olgu sunumları aşağıdaki sıraya göre hazırlanmalıdır

- Başlık sayfası
- Öz (özet)
- Abstract
- Giriş
- Olgu sunumu
- Tartışma
- Teşekkür
- Kaynaklar
- Yazar sayısı en fazla 5 kişi olmalıdır.
- Öz ve Abstract 100-250 kelime olmalıdır.
- Metnin tamamı (Türkçe ve İngilizce özetler dahil, kaynaklar hariç) 2500 kelimeyi aşmamalıdır.
- Olgu sunumlarında hastalardan "Bilgilendirilmiş onam" (informed constent) alınmalıdır ve hastanın kimliği saklı tutulmalıdır.
- Araştırmaya finansman/katkı sağlayan kuruluş ya da kişilere yapılacak teşekkür tartışma ile kaynaklar arasında yer almalıdır.
- Kaynaklar en fazla 15 adet olmalıdır.

Derleme yazıları

- Başlık sayfası bulunmalıdır.
- Yazar sayısı en fazla 3 kişi olmalıdır.
- Öz ve abstract 250-400 kelime olmalıdır.
- Metnin tamamı (Türkçe ve İngilizce özetler dahil, kaynaklar hariç) 5000 kelimeyi aşmamalıdır.
- Kaynaklar en fazla 80 adet olmalıdır.

Editöre mektup
- Başlık sayfası bulunmalıdır.
- Yazar sayısı en fazla 3 kişi olmalıdır.
- Metnin tamamı (kaynaklar hariç) 750 kelimeyi aşmamalıdır.
- Kaynaklar en fazla 10 adet olmalıdır.

Başlık sayfası aşağıdaki içerikte olmalıdır: (Başlık sayfası Araştırma yazıları, Kısa bildiriler, Olgu sunumları, Derleme yazıları ve Editöre mektup'ta bulunmalıdır.)

- Türkçe başlık
- İngilizce başlık
- Yazar isimleri (Sorumlu yazar belirtilmeli)
- Yazarların akademik unvanları
- Yazarların çalıştıkları kurum adresleri
- Yazarların e-posta adresleri
- Sorumlu yazara ait ilave tel, fax numaraları

Öz (Özet) ve Abstract

Tüm yazılarda Türkçe ve İngilizce öz (özet) bulunmalıdır. Türkçe ve İngilizce özler (özet) Araştırma yazıları için 150-400 kelime, Kısa bildiriler için 150-400 kelime, Olgu sunumları için 100-250 kelime, Derleme yazıları için 250-400 kelime olmalıdır. Özlerin hemen altında Türkçe ve İngilizce en az üç en fazla beş kelimeden oluşan "Anahtar Kelimeler" bulunmalıdır. "Anahtar Kelimeler" Türkiye Bilim Terimleri'nden (http://www.bilimterimleri.com) seçilmelidir. Türkiye Bilim Terimleri; MeSH (Medical Subject Headings) terimlerinin, Türkçe karşılıklarını içeren anahtar kelimeler dizinidir.

Kaynaklar

Referansların doğruluğundan yazarlar sorumludur. Kullanılan kaynaklar, cümlelerin sonunda parantez içinde rakamlarla belirtilmelidir. Yazının "Kaynaklar Bölümü" ise yazının en son kısmında yer almalı ve kaynaklar yazıda geçiş sırasına göre sıralanmalıdır. Kaynaklar, yazarların soyadlarını ve adlarının baş harflerini, yazının başlığını, derginin adını, başlangıç ve bitiş sayfaları ile basım yılını içermelidir. Altıdan fazla yazarı olan yazılarda, ilk üç yazardan sonrası için 've ark.' veya 'et al.' ifadesi kullanılmalıdır. Kısaltmalar Index Medicus'a uygun olmalıdır.
Örnekler
Dergide çıkan yazılar için kaynak yazım şekli:
Stephane A. Management of congenital cholesteatoma with otoendoscopic surgery: case report. Türkiye Klinikleri J MedSci 2010;30(2):803-7.
* Türkiye'de yayımlanan dergilerin adları (PubMed'de indekslenenler hariç) tam olarak yazılmalıdır.

Kitap için kaynak yazım şekli
Dieffenbach CW, Dveksler GS (Edited by). PCR Primer. 2nd Edition, New York: Cold Spring Harbor Laboratory Press, 2003:107-108.

Kitaplardaki bölümler için kaynak yazım şekli
Dieffenbach CW, Dveksler GS (Edited by). PCR Primer. In: Roux KH. Optimization and Troubleshooting in PCR. 2nd Edition, New York: Cold Spring Harbor Laboratory Press, 2003:35-41.

On-Line yazı için kaynak yazım şekli
Ticari olmayan ve hükümetler ile ulusal ve uluslararası bilimsel kurul ve kuruluşların resmi internet sayfaları, erişim tarihi belirtilerek kaynak olarak gösterilebilir.
Kavuncu V, Evcik D. Physiotherapy in rheumatoid arthritis. http://www.medscape.com/viewarticle/474880?src=search Erişim 20.05.2004.

Tezler için kaynak yazım şekli
Arıkan Terzi ES. RORA, ROBO1, CFH ve HTRA1 Gen polimorfizmlerinin Yaşa Bağlı Makula Dejenerasyonu ile ilişkisinin araştırılması. Doktora Tezi. Afyonkarahisar: Afyon Kocatepe Üniversitesi Tıp Fakültesi, Tıbbi Genetik Anabilim Dalı, 2014.

İletişim
Dergi Asistanı: R. Buğra HÜSEMOĞLU
Dokuz Eylül Üniversitesi, Sağlık Bilimleri Enstitüsü, Biyomekanik Anabilim Dalı
e-mail: bugrahusem@gmail.com

Editör Sekreteri: Yeşim ÇELİKKANAT
Adres: Osmangazi Tıp Dergisi, Eskişehir Osmangazi Üniversitesi Tıp Fakültesi, 26480 Eskişehir, Türkiye
Tel: +90 222 239 29 79 / 4489
Fax: +90 222 239 37 72
e-Posta: info@jomit.org
otd@ogu.edu.tr

Dergi web sayfası: www.jomit.org

Basımevi:Eskişehir Osmangazi Üniversitesi Basımevi
Adres: Eskişehir Osmangazi Üniversitesi Meşelik Yerleşkesi, Eskişehir
Tel: +90 222 239 37 50 / 3105
e-mail: esogugrafik@gmail.com

İçindekiler / Contents

JOURNAL OF MEDICAL INNOVATION AND TECHNOLOGY VOLUME 3 - ISSUE 2

Research Articles / Araştırma Makaleleri

Reviews / Derlemeler

Research Article

An in vitro assessment of the responses of human dermal fibroblast seeded on 3D printed thermoplastic polyurethane scaffold

3B Baskılı termoplastik poliüretan iskeleye ekilen insan dermal fibroblast yanıtlarının in vitro değerlendirilmesi

Ufkay Karabay [1,2], Selma Aydemir[3], Mehtap Yuksel Egrilmez[1], Basak Baykara[3], R. Bugra Husemoglu[4]

[1]Department of Molecular Medicine, Institute of Health Sciences Dokuz Eylul University, Izmir, Turkey

[2]Department of Pathology Laboratory Techniques, Vocational School of Health Services, Izmir Tinaztepe University, Izmir, Turkey

[3]Department of Histology and Embryology, Faculty of Medicine, Dokuz Eylul University, Izmir, Turkey

[4]Department of Biomechanics, Institute of Health Sciences, Dokuz Eylul University, Izmir, Turkey

Abstract

Tissue engineering is a multidisciplinary field is an interdisciplinary field for the design of biological substitutes that can improve, restore, and maintain tissue functions. Thermoplastic polyurethanes (TPUs) are linear polymers which are widely used for tissue engineering due to its flexibility in processing methods, biocompatibility and excellent mechanical properties. They are suitable materials for use in three-dimensional (3D) printing. Dermal fibroblasts are mesenchymal cells which play crucial roles in physiological tissue repair. The present study aimed to investigate the viability, proliferation, adhesion, and type IV collagen expression of human dermal fibroblasts (HDFs) seeded on 3D printed TPU scaffolds in vitro. HDFs were seeded on 3D TPU scaffolds or tissue culture polystyrene plates as control and cultured for 1, 3, 7, and 14 days. 3D TPU scaffolds were prepared using a custom made fused deposition modelling printer. The viability and proliferation of cells was analyzed by WST-1 assay on days 1 and 3. The cell adhesion was evaluated by scanning electron microscopy (SEM) on days 1 and 3. The cell morphology was examined by hematoxylin and eosin (H&E) staining. Expression of type IV collagen was analyzed by immunohistochemical (IHC) staining. The viability of HDFs on 3D TPU scaffolds was lower than their control groups on days 1 and 3, slightly higher on day 3. SEM images showed HDF attachment to the 3D TPU scaffold surface with spindle-shaped morphology. H&E staining demonstrated that HDFs on 3D TPU scaffolds showed smaller morphologies on days 7 and 14 compared to days 1 and 3. Type IV collagen staining was more intense in HDFs on 3D TPU scaffolds on day 1, 3, and 7 compared to day 14. In conclusion, our study shows the biocompatibility and the potential applications of 3D printed TPU scaffolds for skin tissue engineering using fibroblasts.

Keywords: TPU, human dermal fibroblast, scaffold

Özet

Doku mühendisliği, doku fonksiyonlarını iyileştirebilen, restore edebilen ve sürdürebilen biyolojik ikamelerin tasarımı çalışmalarını içeren multidisipliner bir alandır. Termoplastik poliüretanlar (TPU'lar), üretim yöntemlerindeki esneklikleri, biyouyumlulukları ve mükemmel mekanik özellikleri nedeniyle doku mühendisliğinde yaygın olarak kullanılan lineer polimerlerdir. Bu özellikleri ile üç boyutlu (3B) baskıda kullanıma uygun malzemelerdir. Dermal fibroblastlar (HDF), fizyolojik doku onarımında önemli rol oynayan mezenkimal hücrelerdir. Çalışmamızda, in vitro olarak 3B baskılı TPU doku iskelelerine ekilen insan HDF'lerin canlılığı, proliferasyonu, adezyonu ve tip IV kollajen ekspresyonunu araştırmayı amaçladık. HDF'ler, 3B TPU doku iskeleleri ve kontrol olarak doku kültürü polistiren plakaları üzerine ekildi ve 1, 3, 7 ve 14 gün boyunca kültüre edildi. 3B TPU doku iskeleleri, özel yapılmış bir eriyik yığma modelleme (FDM) yazıcısı kullanılarak hazırlandı. Hücrelerin canlılığı ve proliferasyonu, 1. ve 3. günlerde WST-1 testi ile analiz edildi. Hücre adezyonu, 1. ve 3. günlerde taramalı elektron mikroskobu (SEM) ile değerlendirildi. Hücre morfolojisi, hematoksilen ve eozin (H&E) boyaması ile incelendi. Tip IV kollajen ekspresyonu, immünohistokimyasal (IHC) boyama ile analiz edildi. HDF'lerin 3B TPU doku iskeleleri üzerindeki canlılığı, 1. ve 3. günlerde kontrol gruplarından daha düşük, 3. günde biraz daha yüksekti. H&E boyaması ile, 3B TPU doku iskelelerindeki HDF'lerin 1. ve 3. günlere kıyasla 7. ve 14. günlerde daha küçük morfolojiler gösterdiği tespit edildi. Tip IV kollajen boyaması, 3B TPU doku iskelelerindeki HDF'lerde 14. güne kıyasla 1., 3. ve 7. günlerde daha yoğundu. Sonuç olarak, çalışmamız, cilt dokusu mühendisliği için 3B baskılı TPU doku iskelelerinin fibroblastlar ile biyouyumluluğunu ve potansiyel uygulamalarını göstermektedir.

Anahtar Kelimeler: TPU, insan dermal fibroblast, doku iskelesi

Correspondence Address : R.Bugra Husemoglu, Department of Biomechanics, Institute of Health Sciences, Dokuz Eylul University, Izmir, Turkey
bugrahusem@gmail.com

ORCID ID of the author: U.K 0000-0001-8608-1865, S.A 0000-0003-1263-9998, M.Y.E 0000-0002-3570-1865, B.B 0000-0002-4178-2235, R.B.H 0000-0003-1979-160X

Please cite this article in press at: Karabay U., Aydemir S., Egrilmez M.Y., Baykara B., Husemoglu R. B., An in vitro assessment of the responses of human dermal fibroblast seeded on 3D printed thermoplastic polyurethane scaff, Journal of Medical Innovation and Technology, 2021; 3 (2): 23-27 doi 10.51934/jomit.1049419

1.Introduction

Dermal fibroblasts are cells of mesenchymal origin that play a key role in skin homestasis. They secrete extracellular matrix (ECM) and provide a physical support for other cells to perform their biological functions (1). They are critical in supporting physiological tissue repair (2). Impaired wound healing is commonly associated with comorbidity characteristics, such as diabetes, obesity and autoimmune diseases (3). One of the most promising wound healing approaches involves cell seeded-scaffolds. A scaffold is typically used to provide structural support for cell attachment, differentiation, proliferation and migration (4). Three-dimensional (3D) printed constructs are suitable candidates to provide a biomimetic structural environment that facilitates accelerated wound healing (5).

Thermoplastic polyurethanes (TPUs) are linear segmented block polymers containing hard segments and soft segments (6). They are characterized by high biocompatibility, biodegradability, moderate bending strength and resistance to abrasion (7). Properly designed TPUs are suitable materials for use in 3D printing by the fused deposition modeling (FDM) [8].

In an engineered in vitro model, the scaffold should be designed to replicate in vitro the architecture of the native tissue. Cell infiltration and inflammatory response are essential for sufficient remodeling and successful tissue regeneration of an implanted degradable material. Dermal fibroblasts are commonly used in 3D printed tissue scaffolds of different biomaterials for tissue engineering applications. The constantly growing areas of application make the optimization of TPU materials indispensable.

In this study, we aimed to investigate the viability, proliferation, adhesion, and type IV collagen expression of human dermal fibroblasts (HDFs) seeded on 3D printed TPU scaffolds in vitro.

2.Materials and Methods

Cell culture

Adult HDFs were obtained from ATTC (USA). They were cultured using fibroblast growth medium at 37°C in a humidified atmosphere containing 5% CO2. When the cells were 90% confluent, they were trypsinized and seeded on 3D printed TPU scaffolds. Cells were used between 5-6 passages.

Fabrication of 3D printed TPU scaffolds

Scaffolds template (Ø = 4 mm, thickness = 2 mm) were designed using SolidWorks 2019 software and subsequently filled and sliced using and Ultimaker Cura 4.11 software to obtain cylindrical STL models. Briefly, clump generator software was used to create squared pores into a 3D object in a "stl" □le format. 3D-printed scaffolds were prepared from TPU (eSun Filament, Shenzhen, China). The 3D printer was a customized system working by the mechanism of FDM. Printing was performed by the custom made FDM printer, using a nozzle diameter of 0.4 mm, a layer thickness of 0.2 mm, a nozzle temperature of 240 °C TPU, and a printing bed temperature of 40°C. All scaffolds had a thickness of 2 mm. Both layers were printed with three perimeter lines and rectilinear filling under an angle of 0-90°, applying a flow rate of 100%. Printing speed was set to be 60 mm/s for all materials. Prior to biological evaluations, printed scaffolds were sterilized by ethylene oxide.

Cell Seeding on 3D printed TPU scaffolds

Sterile 3D TPU scaffolds were immersed in fibroblast growth medium in the 96-well plate. Then, they were incubated overnight in a humidified incubator at 37°C with 5% CO2 prior to cell seeding. Suspension of HDFs in fibroblast growth medium were seeded on the 3D printed TPU scaffolds at 4x104 cells per well and incubated for 4 h to allow cell attachment. Each well was completed to 150 µL complete medium in total volume. In order to eliminate the cells that do not attach to scaffolds, 16-24 hours after seeding the scaffolds were placed in another 96-well plate. HDFs with equivalent numbers were also seeded on tissue culture polystyrene plates without scaffolds as a control group. 3D TPU scaffolds were cultured for 1 and 3 days.

Measurement of viability and proliferation on 3D printed TPU Scaffolds

The viability of HDFs on 3D TPU scaffolds was determined by ready-to-use colorimetric WST-1 assay (Biovision, USA). The assay is based upon the cleavage of the tetrazolium salt WST-1 to formazan by cellular mitochondrial dehydrogenases. The amount of formazan dye produced was measured at 450 nm by using a microplate reader (Biotek Synergy HTX, USA). The cell viability of the control group was accepted as 100% and the relative cell viability was calculated respect to this value.

Scanning electron microscopy

The adhesion and the morphology of HDFs on 3D TPU scaffolds were examined by scanning electron microscopy

(SEM). The cells were cultured for 1 and 3 days on 3D TPU scaffolds. Then, the cell-scaffolds constructs were transferred to the 24-well plate, fixed with 4% paraformaldehyde and immersed in a graded series of ethanol (60%, 70%, 80% and 99% v/v). The scaffolds were wrapped in aluminum foil and dried in the desiccator for 2 days (8). The scaffolds placed on the platform were plated with 5 nm gold for 20 minutes by the Q150R S (Quorum) instrument. Copper banding was then applied to the platform to eliminate charging effect. Images were taken by ZEISS Sigma 500 VP FE-SEM.

Histological staining

HDFs on 3D TPU scaffolds were cultured for 1, 3, 7, and 14 days. Cell-scaffold constructs were removed, washed three times in PBS and fixed in 4% paraformaldehyde at 4 °C for 24 h. This was followed by a tissue processing procedure, embedded in paraffin and cut into 5 µm thick sections. The sections were then stained with hematoxylin & eosin (H&E) and were examined under light microscope (Olympus, BX51 microscope) (9). In immunohistochemical (IHC) evaluation, 5 µm thick sections were treated with type IV collagen antibody (bs 10423R, Bioss) and incubated at 4°C for overnight. Antigenic sites were visualized by diaminobenzidine solution and counterstained with hematoxylin. The images were taken with a light microscope (Olympus BX51 microscope) with X20 magnification (10, 11).

Statistical analysis

Statistical analyses were performed using SPSS 24 software program. The results were expressed as mean ± SD. Two groups were compared using Mann Whitney U test. A value of $p<0.05$ was considered significant.

3.Results

The viability and proliferation of HDFs on 3D TPU Scaffolds

The number of HDFs on the 3D TPU scaffolds showed a decrease on day 1 compared to control cells on tissue culture plastic plates without scaffolds ($p<0.05$) (Figure 1A). On day 3, the number of HDFs on the 3D TPU scaffolds were still lower than the control cells. However, the number of cells showed a tendency to increase on day 3 showing cell poliferation ($p<0.05$) (Figure 1B).

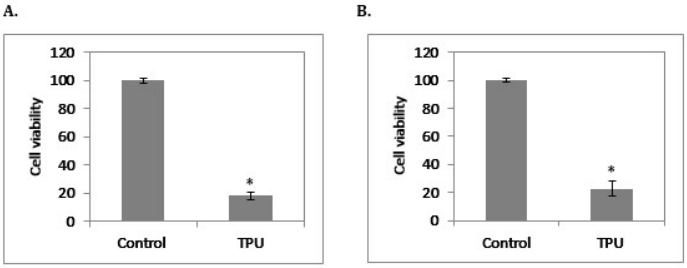

Figure 1. The viability and proliferation of HDFs on 3D TPU scaffolds on day 1 (A) and day 3 (B). * p□ 0.05 in comparison with control.

The morphology of HDFs on 3D TPU scaffolds

We vizualized whether HDFs were capable of adhering to 3D TPU scaffolds via SEM. HDFs adhered to the surfaces of 3D TPU scaffolds, filled the interfiber gaps and maintained their spindle-shaped morphology on days 1 and 3. The cell-cell and cell-scaffold interactions increased on day 3 compared to day 1 showing the biocompatibility of the 3D TPU scaffolds (Figure 2).

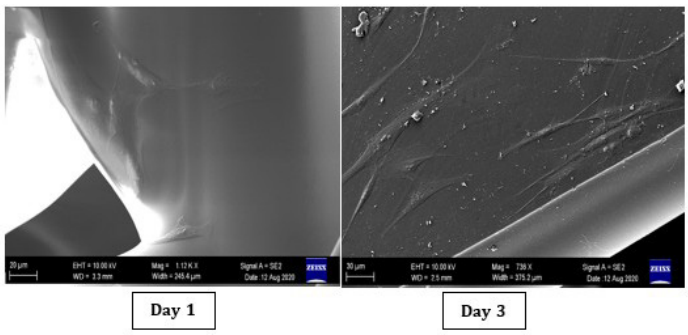

Figure 2. SEM images of HDFs on 3D TPU scaffolds on days 1 and 3.

Histological analysis

H&E staining demonstrated that HDFs attached to 3D TPU scaffolds in on days 1, 3, 7, and 14. We found that HDFs on 3D TPU scaffolds showed smaller morphologies on days 7 and 14 compared to days 1 and 3. The adherence and proliferation of HDFs seeded on 3D TPU scaffolds on day 14 were lower than days 1, 3, and 7 (Figure 3).

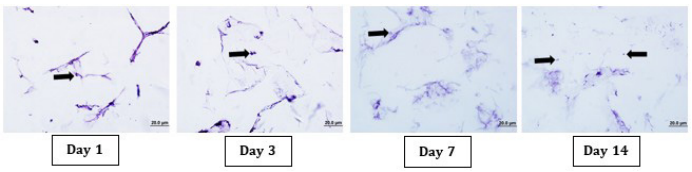

Figure 3. H&E staining in HDFs seeded on 3D TPU scaffolds on days 1, 3, 7, and 14. Black arrows indicate HDFs.

Type IV collagen expression was observed in HDFs on 3D TPU scaffolds on days 1, 3, 7, and 14. Type IV collagen staining in HDFs on 3D TPU scaffolds was moderate and similar on days 1, 3, and 7. However, type IV collagen staining was less intense on day 14 compared to other days (Figure 4).

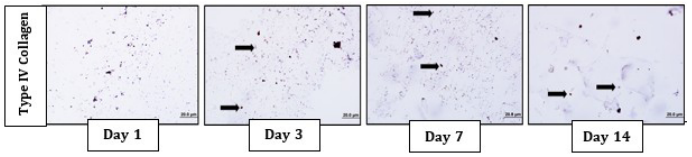

Figure 4. Type IV collagen staining in HDFs seeded on 3D printed TPU scaffolds on days 1, 3, 7, and 14. Black arrows indicate stained HDFs.

4.Discussion

The aim of this study was to investigate the biocompatibility of 3D printed TPU scaffolds by using HDFs in vitro. The viability, adhesion, proliferation, and type IV collagen expression of HDFs seeded on the 3D TPU scaffolds were analyzed.

3D printing is the state-of-the-art technology for tissue engineering applications. The development of 3D printed polymer scaffolds provides control of the architecture and allowing to study the effects of the geometry in cellular responses (13). TPU is a linear polymer consists of polar hard and nonpolar soft segments. They are mainly used because of its biocompatibility, high fracture strain, adequate tensile strength and abrasion resistances (14).

Dermal fibroblasts are instrumental in the physiological tissue repair. SEM images showed that HDFs adhered to the surfaces of 3D printed TPU scaffolds and showed spindle-shaped morphology on days 1 and 3. This result shows the biocompatibility of the 3D TPU scaffolds in terms of adherence in HDFs. The number of HDFs on the 3D TPU scaffolds showed a decrease on days 1 and 3 compared to control group. However, the cell number tended to increase on day 3, resulting a slightly higher cell viability compared to day 1. 3D TPU scaffolds with soft properties were used in this study. Mi et al showed that the number of 3T3 fibroblasts on TPU scaffolds with soft properties were lower than the number of cells on TPU scaffolds with hard properties (15). Another study also reported that the number of human monocytes on soft TPU scaffolds were lower than the number of cells on hard TPU scaffolds (16). Our low cell viability results for HDFs on soft TPU scaffolds are similar with these previous studies.

H&E staining showed that HDFs attached to 3D TPU scaffolds on days 1, 3, 7, and 14. They were found to be in smaller morphologies on days 7 and14 compared to days 1 and 3. The adherence and proliferation of HDFs seeded on 3D TPU scaffolds on day 14 were lower than days 1, 3, and 7. Type IV collagen is primarily found in the skin within the basement membrane zone (17). Olsen et al showed the expression of type IV collagen in HDFs (18). Betz et al emphasized the importance of type IV collagen expression in wound healing (19). In our study, type IV collagen expression was observed in HDFs on 3D printed TPU scaffolds on days 1, 3, 7, and 14. Type IV collagen staining in HDFs on 3D TPU scaffolds was moderate and similar on days 1, 3, and 7. However, type IV collagen staining was less intense on day 14 compared to other days. These histological observations demonstrated the presence of HDFs on 3D TPU scaffolds and the attachment of HDFs to these scaffolds.

5. Conclusion

Our present study assessed the responses of HDFs seeded on 3D printed TPU scaffolds in vitro. Overall, our results show the biocompatibility and the potential applications of 3D printed TPU scaffolds for skin tissue engineering using fibroblasts.

References

1. Haniffa MA, Wang X-N, Holtick U, Rae M, Isaacs JD, Dickinson AM, Hilkens CMU, Collin MP. Adult human fibroblasts are potent immunoregulatory cells and functionally equivalent to mesenchymal stem cells. J Immunol 2007;179:1595-1604.

2. Forrest, L. Current concepts in soft connective tissue wound healing. Br J Surg 1985;70:133-40.

3. Negut I, Dorcioman G, Grumezescu V. Scaffolds for wound healing applications. Polymers (Basel), 2020;12: 2010.

4. Behere I, Ingavle G. In vitro and in vivo advancement of multifunctional electrospun nanofiber scaffolds in wound healing applications: Innovative nanofiber designs, stem cell approaches, and future perspectives. J Biomed Mater Res A 2022;110:443-61.

5. Richards DJ, Tan Y, Jia J, Yao H, Mei Y. 3D Printing for tissue engineering. Isr J Chem. 2013;53:805-14.

6. Harynska A, Kucinska-Lipka J, Sulowska A, Gubanska I, Kostrzewa M, Janik H. Medical-Grade PCL based polyurethane system for FDM 3D Printing-Characterization and Fabrication. Materials (Basel). 2019 Mar 16;12:887.

7. Joseph J, Patel RM, Wenham A, Smith JR. Biomedical applications of polyurethane materials and coatings. Trans Inst Met Finish. 2018;96:121-29.

8. Xiao J, Gao Y. The manufacture of 3D printing of medical grade TPU. Prog Addit Manuf 2017; 2: 117-23.

9. Farrugia BL, Brown TD, Upton Z, Hutmacher DW, Dalton PD, Dargaville TR. Dermal fibroblast infiltration of poly(ε-caprolactone) scaffolds fabricated by melt electrospinning in a direct writing mode. Biofabrication. 2013;5: 025001.

10. Huerta RR, Silva E, Ekaette I, El-Bialy T, Saldaña MDA. High-Intensity ultrasound-assisted formation of cellulose nanofiber scaffold with low and high lignin content and their cytocompatibility with gingival fibroblast cells. Ultrason Sonochem 2020;64:104759.

11. Chen WC, Wei YH, Chu IM, Yao CL. Effect of chondroitin sulphate C on the in vitro and in vivo chondrogenesis of mesenchymal stem cells in crosslinked type II collagen scaffolds. J Tissue Eng Regen Med 2013;7:665-72.

12. Griffin MF, Naderi N, Kalaskar DM, Seifalian AM, Butler PE. Argon plasma surface modification promotes the therapeutic angiogenesis and tissue formation of tissue-engineered scaffolds in vivo by adipose-derived stem cells. Stem Cell Res Ther 2019;10:1-14.

13. Hollister SJ. Porous Scaffold Design for Tissue Engineering. Nature Materials 2005;4:518-24.

14. Tatai L, Moore TG, Adhikari R, Malherbe F, Jayasekara R, Griffiths I, Gunatillake PA. Thermoplastic biodegradable polyurethanes: The effect of chain extender structure on properties and in-vitro degradation. Biomaterials 2007;28:5407-17.

15. Mi HY, Jing X, Salick MR, Cordie TM, Peng XF, Turng LSh. Properties and fibroblast cellular response of soft and hard thermoplastic polyurethane electrospun nanofibrous scaffolds. J Biomed Mater Res B Appl Biomater . 2015;103:960-70.

16. Woitschach F, Kloss M, Schlodder K, Borck A, Grabow N, Reisinger EC, Sombetzki M. In vitro study of the interaction of innate immune cells with liquid silicone rubber coated with zwitterionic methyl methacrylate and thermoplastic polyurethanes. Materials 2021;14:5972.

17. Hasegawa H, Naito I, Nakano K, Momota R, Nishida K, Taguchi T, et al. The distributions of type IV collagen alpha chains in basement membranes of human epidermis and skin appendages. Arch Histol Cytol 2007;70:255-65.

18. Olsen DR, Peltonen J, Jaakkola S, Chu ML, Uitto J. Collagen gene expression by cultured human skin fibroblasts. Abundant steady-state levels of type VI procollagen messenger RNAs. J Clin Invest 1989;83(3): 791-5.

19. Betz P, Nerlich A, Wilske J, Tübel J, Wiest I, Penning R, et al. The time-dependent rearrangement of the epithelial basement membrane in human skin wounds-immunohistochemical localization of Collagen IV and VII. Int J Legal Med 1992;105:93-7.

Research Article

Radiological Evaluation of the Effects of Printing Parameters on 3D Printed Cylindrical LW-PLA Samples: Preliminary Results

3 Boyutlu Baskı Parametrelerinin Silindirik LW-PLA Baskıları Üzerindeki Etkilerinin Radyolojik Değerlendirmesi: İlk Bulgular

İsmail Özsoykal[1], R. Buğra Hüsemoğlu[2], Ayşegül Yurt[1]

[1]Dokuz Eylul University, Health Sciences Institute, Medical Physics Department, Izmir, Turkey.

[2] Dokuz Eylul University, Institute of Health Sciences, Department of Biomechanics, Izmir, Turkey

Abstract

Purpose: In this study, it is aimed to evaluate the radiological tissue equivalency of different 3D printed samples obtained at different printing temperatures, flow rates and infill rates.

Materials and Methods: Ultimaker 3 Extended 3D printer and LW-PLA filament were used witin the scope of this study. A total of 18 cylinders were printed by using 3 different printing temperatures of 195°C, 200oC and 205oC, 3 different flow rates of 60%, 80% and 100%, and 2 different infilling rates of 90% and 100%. Each sample is obtained 1 cm in diameter and 3 cm in height. After calculating the densities of the samples, they were imaged by a Philips Brilliance 128-slice computed tomography scanner. In the images, the average Hounsfield Unit values and the standard deviations of these values were recorded at 5 different axial positions for each sample. The mean HU and standard deviation values recorded over 5 slices were evaluated according to the printing parameters.

Results: Density of the samples are obtained between 0.63 g/cm3 and 1.19 g/cm3. It was observed that the density of the samples were directly proportional to the flow rate and the infill rate. In addition, the average Hounsfield Unit values of the samples varied between -450 and +73. On the other hand, the standard deviation values were recorded between ±6 and ±25. It was observed that the mean Hounsfield Unit values increased with increasing temperature, flow rate and infill rate. The standard deviation values decreased with increasing printing temperatures.

Conclusion: Considering the mean Hounsfield Unit values of different tissues imaged in routine computed tomography examinations, it is concluded that the samples obtained at different printing parameters using LW-PLA filament may have radiological properties that can represent many soft tissues.

Keywords: Computed tomography, 3D printer, radiology

Özet:

Amaç: Bu çalışmada 3 boyutlu yazıcıyla farklı sıcaklıklarda, akış oranlarında ve dolgu oranlarında elde edilen örnek baskıların radyolojik özellik bakımından doku eşdeğerliklerinin değerlendirilmesi amaçlanmmıştır.

Gereç ve Yöntem: Çalışma kapsamında Ultimaker 3 Extended marka 3 boyutlu yazıcı ve LW-PLA filament kullanılmıştır. 195oC, 200oC ve 205oC olmak üzere 3 farklı baskı sıcaklığı, %60, %80 ve %100 olmak üzere 3 farklı akış oranı ve %90 ile %100 olmak üzere 2 farklı dolgu oranı kullanılarak toplamda 18 silindir baskı elde edilmiştir. Her bir baskı 1 cm çapında ve 3 cm boyundadır. Elde edilen baskıların yoğunlukları hesaplandıktan sonra Philips Brilliance marka 128 kesitli bilgisayarlı tomografi cihazında görüntüleri alınmıştır. Görüntülerde her bir baskıya ait 5 farklı kesitte ortalama Hounsfield Unit değerleri ve bu değerlerin standart sapmaları kaydedilmiştir. 5 kesit üzerinden alınan ortalama HU ve standart sapma değerleri baskı parametrelerine göre değerlendirilmiştir.

Bulgular: Elde edilen baskılara ait yoğunluk değerleri 0.63 g/cm3 ile 1.19 g/cm3 arasındadır. Yoğunluk değerlerinin akış oranı ve dolgu oranıyla doğrudan ilişkili olduğu gözlenmiştir. Baskılara ait ortalama Hounsfield Unit değerlerinin ise -450 ile +73 arasında değiştiği gözlenmiştir. Buna karşılık standart sapma değerleri ise ±6 ile ±25 arasında kaydedilmiştir. Ortalama Hounsfield Unit değerlerinin artan sıcaklık, akış oranı ve dolgu oranıyla arttığı gözlenmiştir. Standart sapma değerlerinin ise artan baskı sıcaklıklarında azaldığı gözlenmiştir.

Sonuç: Rutin bilgisayarlı tomografi incelemelerde görüntülenen farklı dokulara ait ortalama Hounsfield Unit değerleri düşünüldüğünde, LW-PLA filamenti kullanılarak farklı baskı parametrelerinde elde edilen örneklerin birçok farklı yumuşak dokuyu temsil edebilecek radyolojik özelliklere sahip olabileceği sonucuna ulaşılmıştır.

Anahtar kelimeler: Bilgisayarlı tomografi, 3 boyutlu yazıcı, radyoloji

Correspondence Address : İsmail Özsoykal, Dokuz Eylul University, Institute of Health Sciences, Medical Physics Department Izmir, Turkey ozsoykal@gmail.com

ORCID ID of the author: İ.Ö 0000-0002-5812-9347, R.B.H 0000-0003-1979-160X, A.Y. 0000-0001-9898-2329

Please cite this article in press at: Özsoykal I., Hüsemoğlu R.B.,Yurt A., Radiological Evaluation of the Effects of Printing Parameters on 3D Printed Cylindrical LW-PLA Samples: Preliminary Results, Journal of Medical Innovation and Technology, 2021; 3 (2):28-34 doi: 10.51934/jomit.1037540

1.Introduction

The latest advances in 3D printing technology, including bioprinting, have provided significant contributions to various fields of medical research and practice (1,2). Direct clinical use of 3D printing methods is mainly related to the manufacture of patient specific surgical models, prostheses or even biological tissues. On the other hand, there is an increasing effort to adopt 3D printing technology in radiology and radiation oncology departments for the development of important tools that would help to improve the clinical practice.

Radiology and radiation oncology departmets are equipped with various test objects, named as phantoms, which are used periodically to quantify, evaluate and optimize the performance of imaging (e.g. computed tomography) or radiation therapy (e.g. linear accelerator) devices. By the use of phantoms, image quality or dosimetric accuracy analysis for various irradiation procedures could be carried out without any patient exposed to radiation. Recent studies focus on the use of 3D printing methods such as stereolithography (SLA) or fused deposition modeling (FDM) in the manufacture of various imaging or dosimetry phantoms (3,4).

There are some benchmarks related to the design and manufacture of an imaging or dosimetry phantom. Radiological tissue equivalency, for example, is one of the main targets to accomplish. In order to mimick any part of the body, phantom material is expected to be very similar to a tissue or different tissues of interest, in terms of radiation attenuation properties. Radiological tissue equivalency of phantoms can be analyzed by means of Hounsfield Unit (HU) values obtained in computed tomography (CT) images. Every pixel which builds up a CT image has a HU value which is an indicator of radiation attenuation coefficient of the imaged object. In a CT image, HU values range from -1024 to +3071 for most CT scanners but almost all tissues have HU values between -1000 and +1000 which change depending mostly on the physical density of the tissues (figure 1) (5,6).

There is a number of studies that analyzed the radiological properties of various 3D printed objects (7-18). These studies commonly reported that the physical density and the resulting HU value for a 3D printed object could be modified in two ways, using another filament with different density or changing the infill rate for the printed object. By the date these studies were carried out, other printing parameters such as printing temperature or flow rate have had no influence on the density of the filament at the nozzle outlet. However, for the upcoming years, filament manufacturers started to produce special filaments that are much more sensitive to printing temperature and flow rate which made it possible for the users to reduce the density of a printed object, without reducing the infill rate, by almost 3 times the original filament density.

This study aims to use one of these special filaments and to investigate the influence of printing temperature, flow rate and infill rate on physical density and corresponding HU value of 3D printed objects.

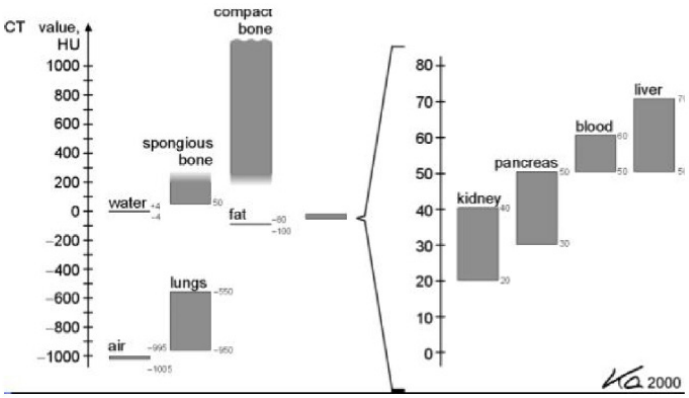

Figure 1. Illustration of the HU values for different tissues in human body (5).

2.Materials and Methods

3D Printing of Samples

In this study, low weight polylactic acid (LW-PLA) based filament (Colorfabb, LW-PLA, Belfeld, Netherlands) was used to print 18 cylindrical samples which were identical in geometry (10 mm diameter and 30 mm height). Cylindrical models have been sliced in Cura which is a 3D printing slicer software for FDM printing. Ultimaker 3 Extended 3D printer was used to obtain the samples (figure 2). The samples were obtained in different printing temperature (195°C, 200°C, 205°C), flow rate (%60, %80, %100) and infill rate (%90, %100) settings while all other basic printing parameters were held constant as shown in table 1.

Table 1. Print settings for 18 different cylindrical samples which were printed at 3 diffferent printing temperature, 3 different flow rate and 2 different infill rate settings.

Print Settings	Adjusted Value
Printing Temperature (°C)	195, 200, 205
Flow Rate (%)	60, 80, 100
Infill Rate (%)	90, 100
Infill Pattern	Grid
Nozzle Diameter (mm)	0.4
Layer Thickness (mm)	0.2
Printing Speed (mm/s)	50
Fan Speed (%)	50

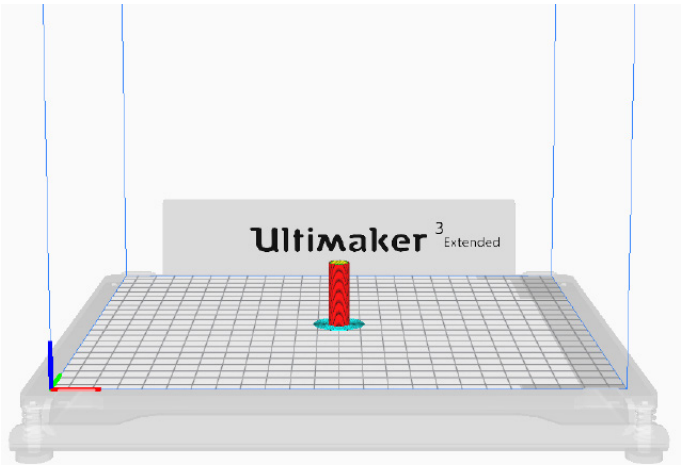

Figure 2: Cylindrical sample which was sliced in Cura software prior to printing in Ultimaker 3 Extended 3D printer.

Physical Density Measurements and Computed Tomography Scan

Physical densities of the printed samples have been determined prior to CT scan. For this purpose, mass and volume of each sample have been measured and calculated by using a microbalance (U.S. Solid, Model USS-DBS00008, Ohio, USA) with a sensitivity of 10-4 grams and a micrometer (Insize Digital Caliper, Model 1112- 200, Suzhou, China) with a sensitivity of 10-3 cm. Then, the samples were placed in a specialized holder which has been stabilized on a polymethylmetacrylate (PMMA) block (figure 3).

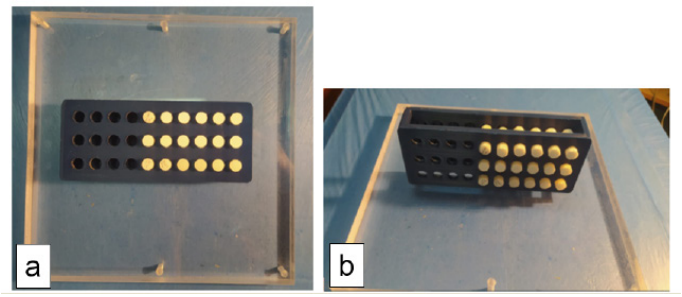

Figure 3: (a)18 cylindrical samples in a holder on a PMMA block and (b) CT imaging setup.

CT scan parameters were selected as shown in table 2. This setup is one of the most frequently used protocols for routine clinical scans. The scanner used for the imaging procedure was Philips Brilliance 128 slice CT scanner which is located in the radiology department of Dokuz Eylul University Research and Application Hospital.

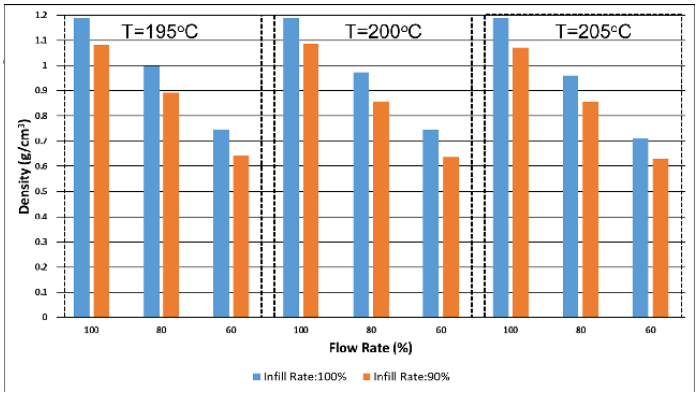

Hounsfield Unit (HU) Analysis of Printed Samples

CT image data has been loaded to imQuest which was developed by Duke University as a practical tool for CT image analysis and made available online (19). Image analysis has been performed over axial slices obtained along the longitudinal axis of cylindrical objects (figure 4). Mean HU values and standard deviation (STD) in HU values have been collected at 5 different positions along the longitudinal (z) axis by drawing circular regions of interest (ROIs) into the central portion of each cylindrical object. In addition, another ROI has been located inside the PMMA block which is assumed to be an adequately homogeneous medium to act as a reference for the evaluation of STD observed in printed samples.

Overall mean HU and STD values for each printed sample have been determined by taking the average of the 5 values collected over 5 different axial measurements. Mean HU values were used to interpret the radiological property of the sample and STD values were used to evaluate the homogeneity of printed samples.

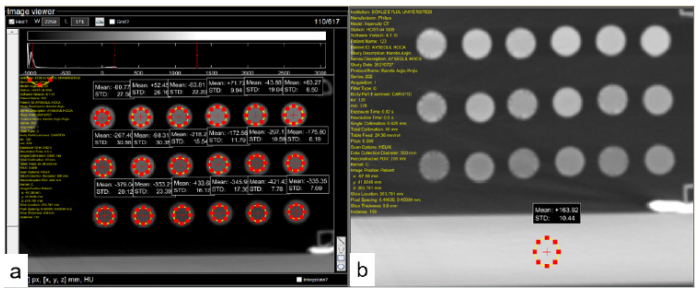

Figure 4: Axial CT images obtained for the measurement of mean HU and standard deviation (STD) values within ROIs of (a) 18 different cylindrical samples and (b) PMMA block.

3. Results

Physical Density Results of Printed Samples

Figure 5 illustrates the results obtained for physical densities of LW-PLA cylinders printed in this study. In general, the samples are found to have different densities ranging between 0.63 g/cm3 and 1.19 g/cm3. Reduction in flow rate and infill rate were observed to result in lower density prints. Furthermore, it is observed that the ratio of decrease observed in the density of samples was very similar to the ratio of reduction in flow rate and infill rate. That is to say, a 20% decrease in flow rate resulted in 20% decrease in density of the printed object. The same relationship is valid for the infill rate as well. On the other hand, printing temperature did not seem to have an influence on physical density as strong as other parameters, since the change is observed to be negligible between 195°C and 205°C.

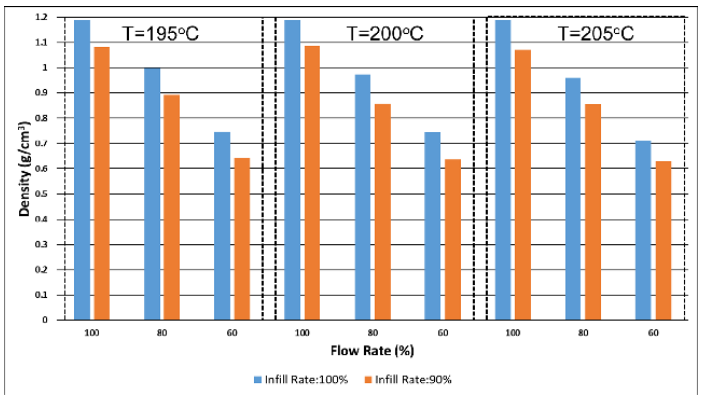

Figure 5: Physical densities of LW-PLA samples printed at different temperatures, flow rates and infill rates.

Hounsfield Unit Analysis of the Samples: Mean HU values and Standard Deviation

Results of mean HU and STD values for the printed samples are given in both table 3 and figure 6. The mean HU values were measured between -450 HU and +73 HU, while STD values were measured between ±6 HU and ±25 HU. In addition, STD value of PMMA block has been measured as ±12 HU.

These results indicated that, increasing printing temperature results in an increase in mean HU for all print settings except for 60% flow rate. On the other hand, STD values were observed to decrease with increasing temperature, regardless of infill rate or flow rate selection. When the flow rate is reduced, mean HU values of the samples exhibited a considerable decrease, similar to the effect observed when reducing the infill rate. STD values, in addition, are observed to increase with reducing infill rate, at 100% flow rate and all printing temperatures. However, at lower flow rates such as 80% and 60% it is observed that the influence of infill rate on the STD values diminished, regardless of printing temperature.

Table 3: Mean HU and STD values of cylindrical samples that are printed at different temperature, flow rate and infill rate settings.

Printing Temperature (°C)	**195**					
Flow Rate (%)	100		80		60	
Infill Rate (%)	100	90	100	90	100	90
Mean HU(±STD)	39(±20)	-90(±25)	-185(±22)	-287(±14)	-345(±15)	-450(±14)
Printing Temperature (°C)	**200**					
Flow Rate (%)	100		80		60	
Infill Rate (%)	100	90	100	90	100	90
Mean HU(±STD)	59(±7)	-80(±15)	-176(±11)	-252(±15)	-345(±12)	-450(±11)
Printing Temperature (°C)	**205**					
Flow Rate (%)	100		80		60	
Infill Rate (%)	100	90	100	90	100	90
Mean HU(±STD)	73(±6)	-60(±13)	-140(±7)	-232(±7)	-328(±7)	-442(±7)

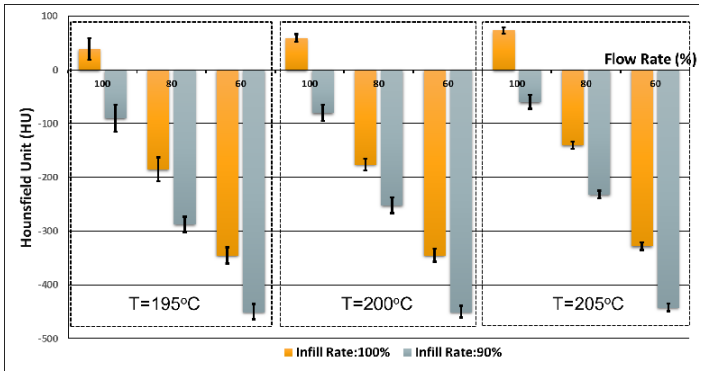

Figure 6: Mean HU and STD values of cylindrical samples printed at different temperature, flow rate and infill rate settings.

4.Discussion

3D printing is a promising technology for a wide range of scientific research. In radiolgy and radiation oncology, adoption of 3D printed tools to help improve clinical practice is an emerging field especially for the last decade (3,4). Phantoms are one of these tools which are used commonly and frequently in the quality control tests of the imaging or radiotherapy modalities. These tests focus on image quality and/or dosimetric accuracy provided by the equipment. For a phantom to be used as such a test tool, it is important to be radiologically tissue equivalent and homogenious.

There are various types of filaments that are used in FDM based 3D printing such as acrylonitrile butadine styrene (ABS), thermoplastic polyurethane (TPU), polylactic acid

(PLA) and high impact polystyrene (HIPS). In addition, some composite filaments that include wood, steel, copper or brass are recently available, widening the advantages of 3D printing for users. Most of these filaments have been used in the studies on radiological properties of 3D printed objects and it is shown that they can cover a range of HU values to correspond to different tissues (7-18). However, as a drawback, those filaments all had specific densities that can not be modified by printing process, i.e. does not change with printing parameters such as temperature and flow rate. The only way to modify density and therefore radiation attenuation property of a printed object is to change the infill rate or the filament itself. Infill rate, however, is not a favorable parameter to modify physical density of a printed object. The reason is that as the infill rate decreases, the distance between any adjecent lines increases and this leads to inhomogeneities in the printed structure which could be beyond the limits to mimick any tissue. Recently, new kind of special filaments are introduced that allow the modification of density of the filament at the nozzle outlet by adjusting printing temperature and flow rate. Such filaments are commercially available since 2019, and to our knowledge, there is not any study published yet in the literature regarding the evaluation of these filaments for radiological purposes. This study is important to introduce the effects of different print settings on the printed objects in terms of radiological tissue equivalency.

The results of this study indicated that the physical density of a printed sample changes depending on all of the three printing parameters. It is shown that the physical density could be reduced approximately by half with the proper selection of print settings (figure 5). Furthermore, it is reported by the manufacturer that it could be reduced by even one third of the original density which is approximately between 1.21 g/cm3 and 1.43 g/cm3. Among all printing parameters, minimum rate of change in density is observed due to printing temperature which is set between 195oC and 205oC. Actually, it is stated by the manufacturer that the foaming, process by which the reduction in density becomes significant, starts at 215 oC. Thus, it can be understood that, below 215oC, the changes in physical density due to printing temperature could be insignificant. Nevertheless, increasing temperature had some significant effects on the mean HU and STD values of the samples as shown in table 3 and figure 6. Especially at high flow rates such as 100% and 80%, it is observed that the samples exhibited a significant increase in mean HU and decrease in STD as a result of higher printing temperature. This could not be due to foaming, but expansion, that can occur increasingly at higher temperatures and lower the volume of air gaps within the sample, thus increasing both the mean HU value and homogeneity (i.e. lower STD) of the printed object.

It is not interesting to observe that the rate of change in physical density has followed to the rate of change in flow rate and infill rate, since both parameters, differently from printing temperature, directly determines the amount of mass that would be deposited in the printed sample. On the other hand, when the influence of these parameters on mean HU is considered, it is observed that mean HU decreases with reduction in both flow rate and infill rate. STD values, in addition, seem to exhibit a higher margin of difference between different infill rates at 100% flow rate, regarding all printing temperatures. However, this difference due to infill rate is observed to diminish, in other words, the homogeneity of the samples became independent of infill rate, as the flow rate became lower. It is also reasonable to state that at high flow rates, the influence of printing temperature on mean HU and STD values are stronger. However at low flow rates this influence becomes insignificant especially for the mean HU values.

In a CT image, different tissues correspond to different HU values ranging between -1000 and +1000 in general. For example, mean HU value is -1000 for air gaps such as nasal cavity and pharynx and around -800 for lungs. For fat and soft tissues it ranges between - 70 to +40, and it is around +1000 for bones or calcified lesions(6). In this study, we obtained cylindrical samples between +73 HU and -450 HU which means that soft tissues such as liver, kidneys, pancreas, stomach, heart and vascular structures could be mimicked. In addition, our results indicated that further reduction in the flow rate and infill rate or increase in printing temperature could help printing samples equivalent to lungs.

In addition to mean HU value, STD value is an important parameter that indicates the homogeneity of the structures in an image. Most tissues have a homogeneous structure with STD values reported to vary between 10%-20% of the mean HU value (6). STD values of the samples printed in this study were in well agreement with this percentage values, except for the samples obtained at 195oC and 100% flow rate. In addition, most of the samples are found to have homogeneities even better than PMMA block. These results suggests the use of 3D printing as a safe tool to design and manufacture of high quality test phantoms for the evaluation of image quality for CT scanners.

There are some limitations to this study. First of all, only one sample was printed per print setting which limited the evaluation of the 3D printing reproducibility and statistical analysis of the results. 5 different axial measurements were taken per sample to overcome this limitation. In addition, samples were obtained from a single 3D printer and a single filament spool. Engagement of multiple printers and multiple spools in the study would contribute to the reproducibility of the results. Another limitation is that the homogeneity of the printed samples was evaluated over the axial planes of the image. However, longitudinal (along the z axis of cylinders) variation should also be considered to assure the stability for the entire volume of the sample. The last limitation is about the range of printing temperature and infill rate used to get the samples. Both parameters meight be extended (i.e. printing temperature can be increased upto 260oC or infill rate can be reduced to lower percentages) to evaluate the results with a wider spectrum of data.

Despite the limitations mentioned above, this study has revealed some notable results. Above all, it is shown that most of the soft tissues could be mimicked by using only one type of filament as a printing material, rather than using a variety of filaments with different densities. Moreover, the influence of the printing temperature and flow rate on both mean HU and STD values is proven to be valueable. Infill rate, on the other hand, is still a helpful print setting to modify density, however it is not very useful when considered by itself, especially due to increasing inhomogeneities at low printing temperatures for which no expansion or foaming of filament is triggered.

5. Conclusion

This study investigated the use of a special filament to obtain radiologically tissue equivalent objects with different densities and radiation attenuation properties. The preliminary results indicated that most of the soft tissues can be mimicked by modifying print settings such as printing temperature, flow rate and infill rate.

Acknowledgements

This study is part of a project which is financially supported by 1005 - National New Ideas And New Products Research Funding Program, TUBITAK. The authors hereby appreciate this opportunity they are provided with.

References

1. Tamay DG, Usal TD, Alagoz AS, Yucel D, Hasirci D, Hasirci V. 3D and 4D Printing of Polymers for Tissue Engineering Applications. Frontiers in Bioengineering and Biotechnology 2019;7:164.

2. C. Lee Ventola. Medical Applications for 3D Printing: Current and Projected Uses. P T. 2014;39(10):704–11.

3. Tino R, Yeo A, Leary M, Brandt M, Kron T. A Systematic Review on 3D-Printed Imaging and Dosimetry Phantoms in Radiation Therapy. Technol Cancer Res Treat. 2019; 18:1533033819870208.

4. Filippou V, Tsoumpas C. Recent advances on the development of phantoms using 3D printing for imaging with CT, MRI, PET, SPECT, and ultrasound. Med Phys. 2018;45(9):e740–60.

5. Kalender WA. Computed tomography: fundamentals, system technology image quality, applications. 3rd edition, Paris: Publicis, 2011.

6. Kamalian S, Lev MH, Gupta AR. Handbook of Clinical Neurology, Neuroimaging Part 1.In: Computed tomography imaging and angiography – principles. Amsterdam: Elsevier, 2016:3-20.

7. Kairn T, Crowe SB, Markwell T. Use of 3D Printed Materials as Tissue-Equivalent Phantoms. In: Jaffray D. (eds) World Congress on Medical Physics and Biomedical Engineering. 2015:728-31.

8. Leng S, Chen B, Vrieze T, et al. Construction of realistic phantoms from patient images and a commercial three-dimensional printer. J. Med. Imag. 2016;3(3): 033501-1-7.

9. Shin J, Sandhu RS, Shih G. Imaging Properties of 3D Printed Materials: Multi-Energy CT of Filament Polymers. J Digit Imaging. 2017;30(5):572-5.

10. Joerner MR, Maynard MR, Rajon DA, Bova FJ, Hintenlang DE. Three-Dimensional Printing for Construction of Tissue-Equivalent Anthropomorphic Phantoms and Determination of Conceptus Dose. AJR. 2018;211(6):1283-90.

11. Alssabbagh M, Tajuddin AA, Abdulmanap M, Zainon R. Evaluation of 3D printing materials for fabrication of a novel multifunctional 3D thyroid phantom for medical dosimetry and image quality. Rad Phys Chem. 2017;135:106-12.

12. Alssabbagh M, Tajuddin AA, Abdulmanap M, Zainon R. Evaluation of nine 3D printing materials as tissue equivalent materials in terms of mass attenuation coefficient and mass density. Int. j. adv. appl. sci. 2017;4(9):168-73.

13. Seoung YH. Evaluation of Usefulness for Quality Control Phantom of Computed Tomography Produced by Using Fused Deposition Modeling 3D Printing Technology. JEAS. 2017;12(12):3137-41.

14. Craft DF, Kry SF, Balter F, Salehpour M, Woodward W, Howell RM. Material matters: Analysis of density uncertainty in 3D printing and its consequences for radiation oncology. Med phys. 2018;45(4):1614-21.

15. Zhang F, Zhang H, Zhao H, et al. Design and fabrication of a personalized anthropomorphic phantom using 3D printing and tissue equivalent materials. Quant Imaging Med Surg. 2019;9(1):94-100.

16. Giron IH, Harder JM, Streekstra GJ, Geleijns J, Weldkamp WJH. Development of a 3D printed anthropomorphic lung phantom for image quality assessment in CT. Phys Med. 2019;57:47-57.

17. Solc J, Vrba T, Burianova L. Tissue-equivalence of 3D-printed plastics for medical phantoms in radiology. JINST. 2018; 13 P09018.

18. Assemany LPF, Junior OR, Silva E, Potiens MPA. Evaluation of 3D printing filaments for construction of a pediatric phantom for dosimetry in CBCT. Rad Phys Chem. 2020;167:108227.

19. imQuest, https://deckard.duhs.duke.edu/~samei/tg233.html. Date of Access:16.12.21

Research Article

Biomechanical Comparison of Different Subtrochanteric Bone Fracture Angles in Cerclage Wiring: Finite Element Study

Serklaj Kablolamada Farklı Subtrokanterik Kemik Kırılma Açılarının Biyomekanik Karşılaştırılması: Sonlu Eleman Çalışması

R. Bugra Husemoglu[1], Hasan Havıtcıoglu[1, 2]

[1] Dokuz Eylul University, Institute of Health Sciences, Department of Biomechanics, Izmir, Turkey

[2] Dokuz Eylül University Faculty of Medicine Hospital, Department of Orthopedics and Traumatology, Izmir, Turkey

Abstract:

Cerclage wires are regularly hired as fixation gear to resource reposition, enhance alignment and growth fixation stability. In specific femoral shaft, subtrochanteric and periprosthetic fractures gain from cerclage fixation. Also in supracondylar femoral shaft fractures, extra cord cerclages proved to be extra than only a reposition device and accelerated the general power of the osteosynthesis construct. This study tests for the stabilizing effect of different bone fracture angles in with cerclage. Cerclage fixation of a oblique fractures were tested with fracture angles (45°, 55°, 65°). Construct stiffness and displacements were investigated under static loads and compared to the different bone fracture angles. With each of the tested bone fractures, stiffness wasn't significantly for a compare angles. Most reduction in fracture gap movement was achieved by 65° fracture angle, followed by 55° and 45° fractures.
All cerclage wire fixation were generally superior with reduced fracture movements whereas in 65 degree fracture showing the greatest stabilizing effect. Cerclage wire application has emerged as a potential therapeutic for subtrochanteric fractures.

Keywords: Oblique Fractures, Cerclage Wire, Bone Fracture Angle, Finite Element Analysis

Özet:

Serklaj telleri, yeniden konumlandırmaya yardımcı olmak, hizalamayı iyileştirmek ve sabitleme stabilitesini artırmak için sabitleme araçları olarak sıklıkla kullanılır. Özellikle femur şaftı, subtrokanterik ve periprostetik kırıklar serklaj fiksasyonundan yararlanır. Ayrıca suprakondiler femur şaft kırıklarında, ek olarak tel serklajların tespit aracından daha fazlası olduğu ve osteosentez yapısının genel mukavvemeti arttırdığı kanıtlanmıştır. Bu çalışma, serklaj ile farklı kemik kırılma açılarının stabilize edici etkisini test etmektedir. Oblik kırıkların serklaj fiksasyonu kırık açıları ile test edildi (45°, 55°, 65°). Yapı rijitliği ve yer değiştirmeler, statik yükler altında incelendi ve farklı kemik kırılma açılarıyla karşılaştırıldı. Test edilen kemik kırıklarının her birinde sertlik, karşılaştırma açılarında anlamlı bulunmadı. Kırık boşluğu hareketindeki en azalma, 65 ° kırılma açısı ile sağlandı, bunu 55° ve 45° kırıklar izledi.
Tüm serklaj teli fiksasyonu, kırık hareketlerini azaltmış ve genel olarak rijit bulunmasının yanında, en büyük stabilize edici etkiyi 65 derecelik kırıkta gösterdi. Serklaj teli uygulaması, subtrokanterik kırıklar için potansiyel bir terapötik olarak ortaya çıkmıştır.

Anahtar Kelimeler: Oblik kırıklar, serklaj kablolama, kemik kırık açısı, sonlu elemanlar analizi

Correspondence Address : R. Buğra Hüsemoğlu, Dokuz Eylul University, Institute of Health Sciences, Department of Biomechanics, Izmir, Turkey bugrahusem@gmail.com

ORCID ID of the authors: R.B.H. 0000-0003-1979-160X, H.H.. 0000-0001-8169-3539

Please cite this article in press at: Husemoglu R.B., Havitcioglu H., Biomechanical Comparison of Different Subtrochanteric Bone Fracture Angles in Cerclage Wiring: Finite Element Study, Journal of Medical Innovation and Technology, 2021; 3 (2):35-39 doi: 10.51934/jomit.1052710

1.Introduction

Cerclage wiring is a simple technique that has been practiced widely since the advent of surgical treatment of fractures. The indications for cerclage as an exclusive implant were limited because other technologies offer a better outcome, while the increasing numbers of periprosthetic fractures has led to a revival of interest for this simple technique.

Cerclage wires have long been used for the fixation of diaphyseal fractures, either alone or in combination with other fixation methods [1]. Cerclage wires are often hired as fixation equipment to useful resource reposition, enhance alignment and increase fixation stability. In particular femoral shaft, subtrochanteric and periprosthetic fractures advantage from supplementary cerclage fixation [2],[3]. Also in supracondylar femoral shaft fractures, extra cord cerclages proved to be extra than only a reposition device and increased the overall strength of the osteosynthesis construct [4].

Cerclage wires are a non-reactive stainless steel alloy, that's a ways extra malleable than the stainless steel alloy used to make bone plates or pins. There are three primary sorts of cerclage wiring, complete cerclage, hemicerclage wiring and tension band wiring, that's a specialized shape of hemicerclage. Full circlage wiring utilizes a full circumferential wire placed around the bone at a fracture site. This use is generally restricted to the diaphyseal segments of long bones. The fracture is carefully reconstructed and the fragments are wired in place prior to applying the definitive form of fixation. Full cerclage anatomic reconstruction of the fracture at the level of the cerclage wire is mandatory, otherwise the fragments will move and collapse and the wire will loosen[5].

Full cerclage wiring is best appropriate for long oblique diaphyseal fractures where the length of the fracture is greater than twice the diameter of the bone at the fracture site (>45°). If the fracture line is greater than two times the diameter of the bone on the fracture site, the wire will acquire inter-fragmentary compression[6].

Finite element (FE) evaluation is a effective biomechanical device that permits for the manage of numerous parameters, such as loading forces, fracture kind and implants, that might in any other case be tough to evaluate in vivo or thru cadaveric experiments.Therefore, in this study, oblique bone fracture angles evaluate their differences using finite element analysis.

2.Materials and Methods

The bone and cerclage wire models was created using the Solidworks software (Dassault Systemes Simulia Corp., Providence, RI, USA). According to the anatomic femur diaphysis based, cylindrical bone specimens were performed. Cylindrical bone samples dimmentions were Ø 30 mm and lenghts 100 mm. Monofilament cerclage wire model created was dimmentions Ø 32 mm and thickness 1.5 mm. In this study, three different bone fracture models were compared. All solid models were imported to analysis software (ANSYS 2020 R1, ANSYS Inc., Houston, TX, USA).

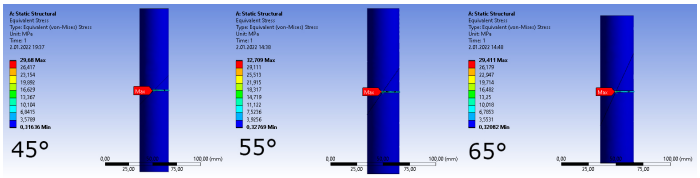

Fig. 1 – Bone specimens and Monofilament Cerclage Wires

Based on the results of the mesh convergence analysis, 2 mm element edge lengths were used for all components. The bone was represented with a single isotropic elastic modulus of 17,000 MPa. A uniform Poisson's ratio of 0.3 was assigned for all bone elements.

A vertical load 800 N, was applied to the proximal. The stress over the cerclage component was evaluated every angle performing a osteotomy. The following material properties were considered for the study as shown in Table 1.

Table 1. Mechanical properties of bone and cerclage wire

Element	Material Properties	Cortical Bone	Cerclage Wire
1.	Young's modulus	17 GPa	186 GPa
2.	Density	2 gm/cm3	1.08 gm/cm3
3.	Poisson's ratio	0.38	0.3

In the present study, the bone was assumed to be as linear isotropic material [7],[8] . The analysis was carried out for loads 800N. The distal end of the bone specimen was constrained in accordance with the previous works [9].

Contact between bone and implant, and between bone fragment was considered to be frictional. The coefficient of friction for the bone-to-bone, bone-to-implant and implant-to-implant contacts were 0.46, and 0.2, respectively [10].

3. Results

Comparison of Bone Fracture Angles

The stress was evaluated proximal at 800 N with for 45° the maximum stress (29,68 MPa), 55 ° the mean stress (32,70 MPa) and for 65° (29,41 MPa) (Table 2)

The maximum stress of the monofilament cerclage wire was at the anterior medial position of the specimen, as shown in Figure 2.

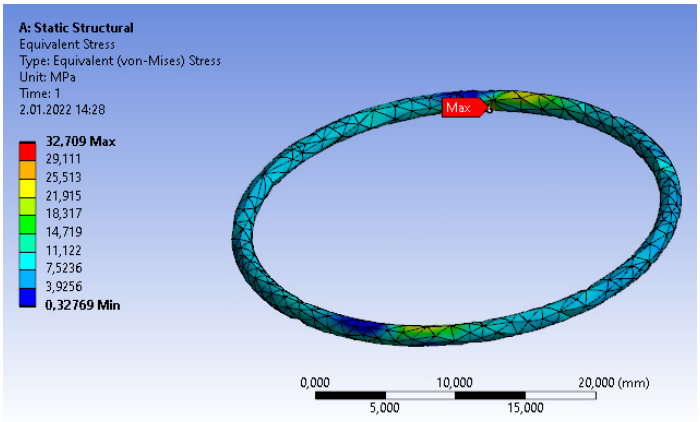

Fig.2 – Maximum Stress of the Monofilament Cerclage Wire

Table 2. Cerclage wire stress values

Fracture Angle	Uzama	Stress (MPa)		
Specimen	Max	Min	Max	Avarage
45°	0,013573	0,31636	29,68	3,0947
55°	0,013043	0,32769	32,709	3,1439
65°	0,011842	0,32082	29,411	3,0909

4.Discussion

This study demonstrates stabilizing effect of angles of fractures on cerclage wiring of oblique fractures. While previous studies focused only on stand-alone cerclage configurations and techniques our study provided a comparison of different bone fracture angle types in a relevant fracture model.

Although augmentation of fracture fixation through cerclages has an enduring tradition and has tested to be clinically successful, its biomechanical implications have now no longer but been explored sufficiently. In addition to its use as a brief percutaneous reduction clamp, a cerclage also can be carried out as an extra stabilization device to enhance the stability of the osteosynthesis.

The bone must have stable anatomical reduction over a complete turn at the level of application or the compression produced by the wire will purpose the bone to collapse or fragment further.

Cerclage wiring is most suited to long oblique fractures where the length of the fracture is greater than two times the diameter of the bone at the fracture site. If the fracture line is greater than two times the diameter of the bone at the fracture site, the wire will achieve inter-fragmentary compression. If the length of the fracture line is much less than two times the bone diameter then shearing forces may be produced on the way to disrupt the fracture [6].

In recent literature, fracture fixation with cerclage wiring is known to be associated with implant-related complications due to secondary fracture displacement and implant migration [11]. Biomechanical studies have revealed that lag screw configurations are stiffer compared with cerclage wiring or cable systems [12], Thus, we were concerned whether the circumferential cerclage would become reduced stiffness during static loading, especially in this idealized 3D bone model. Even 65 degrees bone fracture with loads in excess of physiological loads we were not able to detect too much loosening or migration.

Early weight-bearing regimes are related to decrease hazard of complications, for example better functional outcome at early levels of rehabilitation [13]. Modern fracture care prioritizes rapid return to function as well as patient autonomy and convenience, which can be enhanced by post-operative mobilization and weight-bearing to an extent the patient feels snug with [14].

Some limitations of this study need to be mentioned. Biomechanical in vitro studies have the inherent weakness that in vivo situation. However, it should be noted that the aim was to investigate the clinical trends rather than absolute values. Our load protocols included post-operatively acceptable values for moderate as well as excessive weight-bearing up to 800 N. Cerclage wiring is obviously limited to oblique or spiral fractures and has no further stabilizing effect in transverse or comminuted fractures.

5. Conclusion

The indications for cerclage as an exclusive implant were limited, while this simple technique is frequently used to secure femoral fractures, allografts and plates, especially in periprosthetic fractures. In conclusion, we demonstrated the stabilizing effect of different bone fracture angles cerclage materials.

The findings from this study favor a cable cerclage, as it was able to better reinforce osteosynthesis in terms of higher stiffness and reduced interfragmentary movements. Whether our results can be transferred into the clinical routine has to be investigated in further clinical studies. In this results, bone structure represents the actual femur anatomy and therefore, FEM analysis should take into account the properties of individual layers that constitute the femur for accurate analysis.

References

1. A. Angelini and ▪ Concetto Battiato, "Past and present of the use of cerclage wires in orthopedics," Eur. J. Orthop. Surg. Traumatol.

2. K. Gordon, M. Winkler, T. Hofstädter, U. Dorn, and P. Augat, "Managing Vancouver B1 fractures by cerclage system compared to locking plate fixation - a biomechanical study," Injury, vol. 47 Suppl 2, pp. S51–S57, Jun. 2016.

3. P. Codesido, A. Mejía, J. Riego, and C. Ojeda-Thies, "Subtrochanteric fractures in elderly people treated with intramedullary fixation: quality of life and complications following open reduction and cerclage wiring versus closed reduction."

4. C. Bliemel et al., "More than a reposition tool: additional wire cerclage leads to increased load to failure in plate osteosynthesis for supracondylar femoral shaft fractures," Arch. Orthop. Trauma Surg., vol. 141, no. 7, pp. 1197–1205, Jul. 2021.

5. R. J. Boudrieau and K. R. Sinibaldi, "Principles of long bone fracture management.," Semin. Vet. Med. Surg. (Small Anim)., vol. 7, no. 1, pp. 44–62, 1992.

6. D. P. Akira Takeuchi, "World Small Animal Veterinary Association World Congress Proceedings, 2003," VIN.com, Jul. 2014.

7. "Probabilistic finite element analysis of the uncemented hip replacement—effect of femur characteristics and implant design geometry | Elsevier Enhanced Reader." [Online]. Available: https://reader.elsevier.com/reader/sd/pii/S0021929009005582?token=687D07D3604D056188B9CAB6DDD98FFA96CBA761AB7294C7FBD2885A2544FB6A43D9FD59482B9AC73BF37058C93BEC76&originRegion=eu-west-1&originCreation=20211230094228. [Accessed: 30-Dec-2021].

8. G. E. Cook et al., "Biomechanical optimization of the angle and position for surgical implantation of a straight short stem hip implant," Med. Eng. Phys., vol. 39, pp. 23–30, Jan. 2017.

9. V. M. M. Lopes, M. A. Neto, A. M. Amaro, L. M. Roseiro, and M. F. Paulino, "FE and experimental study on how the cortex material properties of synthetic femurs affect strain levels," Med. Eng. Phys., vol. 46, pp. 96–109, Aug. 2017.

10. J. M. Goffin, P. Pankaj, and A. H. Simpson, "The importance of lag screw position for the stabilization of trochanteric fractures with a sliding hip screw: a subject-specific finite element study," J. Orthop. Res., vol. 31, no. 4, pp. 596–600, Apr. 2013.

11. M. Nienhaus, I. Zderic, D. Wahl, B. Gueorguiev, and P. M. Rommens, "A locked intraosseous nail for transverse patellar fractures: A biomechanical comparison with tension band wiring through cannulated screws," J. Bone Jt. Surg. - Am. Vol., vol. 100, no. 12, p. E83, Jun. 2018.

12. H. S. Matloub, P. L. Jensen, J. R. Sanger, B. K. Grunert, and N. J. Yousif, "Spiral Fracture Fixation Techniques: A biomechanical study," http://dx.doi.org/10.1016/0266-7681(93)90162-9, vol. 18, no. 4, pp. 515–519, Aug. 2016.

13. G. Meys et al., "A protocol for permissive weight-bearing during allied health therapy in surgically treated fractures of the pelvis and lower extremities," J. Rehabil. Med., vol. 51, no. 4, pp. 290–297, 2019.

14. N. Dehghan et al., "Early weightbearing and range of motion versus non-weightbearing and immobilization after open reduction and internal fixation of unstable ankle fractures: A randomized controlled trial," J. Orthop. Trauma, vol. 30, no. 7, pp. 345–352, Jul. 2016.

Research Article

The cellular responses of human macrophages seeded on 3D printed thermoplastic polyurethane scaffold

3B Baskılı termoplastik poliüretan iskeleye ekilen insan makrofajlarının hücresel yanıtları

Mehtap Yuksel Egrilmez[1], Ufkay Karabay [1,2], Selma Aydemir[3], Basak Baykara[3], R. Bugra Husemoglu[4]

[1]Department of Molecular Medicine, Institute of Health Sciences Dokuz Eylul University, Izmir, Turkey

[2]Department of Pathology Laboratory Techniques, Vocational School of Health Services, Izmir Tinaztepe University, Izmir, Turkey

[3]Department of Histology and Embryology, Faculty of Medicine, Dokuz Eylul University, Izmir, Turkey

[4]Department of Biomechanics, Institute of Health Sciences, Dokuz Eylul University, Izmir, Turkey

Abstract: Tissue engineering is an interdisciplinary field for the design of functional constructs that aid to repair damaged or diseased tissue. Three-dimensional (3D) printing is a growing technology that offers new opportunities for tissue engineering. Thermoplastic polyurethane (TPU) is a member of the polyurethane class. TPUs are commonly used in medical applications with their biocompatible, superior mechanical properties and shape memory behavior. Macrophages are key regulators of tissue homeostasis, inflammation, and regeneration. They play crucial roles in initial immune response to implants. In this study, we aimed to investigate the viability, adhesion, and distribution properties of human THP-1 macrophages seeded on 3D printed TPU scaffolds in vitro. The expression of CD68 and CD10 was also analyzed in human THP-1 macrophages on 3D TPU scaffolds. THP-1 macrophages treated with phorbol-12-myristate-13-acetate (PMA) were seeded on 3D TPU scaffolds or tissue culture plastic plates as control and cultured for 1, 3, 7, and 14 days. 3D TPU scaffolds were prepared using a custom made fused deposition modeling printer. The cell viability was measured by WST-1 assay on days 1 and 3. The cell adhesion was evaluated by scanning electron microscopy (SEM). The cell distribution was analyzed by hematoxylin and eosin (H&E) staining. Expression of CD10 and CD68 was analyzed by immunohistochemical (IHC) staining. The viability of THP-1 macrophages on 3D TPU scaffolds was lower than their control groups on days 1 and 3. SEM images showed THP-1 macrophage attachment on the 3D TPU scaffold surface with round and elongated morphologies. H&E staining demonstrated that THP-1 macrophages showed eosinophilic cytoplasm and large nuclei. CD68 staining was more intense in THP-1 macrophages on 3D TPU scaffolds on day 3 compared to days 1, 7 and 14. CD10 staining was more intense on day 1 compared to days 3, 7, and 14. Our results show that 3D TPU scaffolds are biocompatible with macrophages and might be a potential biomaterial for medical applications.

Keywords: macrophages, 3D printed, TPU, cell culture

Özet: Doku mühendisliği, hasarlı veya hastalıklı dokuyu onarmak için destekleyici fonksiyonel yapıların tasarımı için disiplinler arası bir alandır. Üç boyutlu (3B) baskı, doku mühendisliği için yeni fırsatlar sunan ve büyümekte olan bir teknolojidir. Termoplastik poliüretan (TPU), poliüretan sınıfının bir üyesidir. TPU'lar, biyouyumlulukları, üstün mekanik özellikleri ve şekil hafızalı davranışları ile tıbbi uygulamalarda yaygın olarak kullanılmaktadır. Makrofajlar, doku homeostazı, inflamasyon ve rejenerasyonun anahtar düzenleyicileridir. İmplantlara karşı ilk bağışıklık yanıtında çok önemli rol oynarlar. Bu çalışmada, 3B baskılı TPU doku iskelelerine ekilen insan THP-1 makrofajlarının canlılık, adezyon ve dağılım özelliklerini in vitro olarak araştırmayı amaçladık. Ayrıca, 3B TPU doku iskelelerine ekilen insan THP-1 makrofajlarında CD68 ve CD10'un ekspresyonu da analiz edildi. Forbol-12-miristat-13-asetat (PMA) ile uyarılan THP-1 makrofajları, 3B TPU doku iskeleleri ve kontrol olarak doku kültürü plastik plakaları üzerine ekildi ve 1, 3, 7 ve 14 gün boyunca kültüre edildi. 3B TPU doku iskeleleri, özel yapılmış bir eriyik yığma modelleme (FDM) yazıcısı kullanılarak hazırlandı. Hücre canlılığı, 1. ve 3. günlerde WST-1 kiti ile ölçüldü. Hücre adezyonu, taramalı elektron mikroskobu (SEM) ile değerlendirildi. Hücre dağılımı, hematoksilen ve eozin (H&E) boyaması ile analiz edildi. CD68 ve CD10 ekspresyonu, immünohistokimyasal (IHC) boyama ile analiz edildi. THP-1 makrofajlarının 3B TPU doku iskeleleri üzerindeki canlılığı, 1. ve 3. günlerde kontrol gruplarından daha düşük tespit edildi. SEM görüntüleri, THP-1 makrofajların 3B TPU doku iskeleleri yüzeyinde yuvarlak ve uzun morfolojilere sahip olarak tutunduğunu gösterdi. H&E boyaması ile THP-1 makrofajlarının eozinofilik sitoplazma ve büyük çekirdekli morfolojide olduğu gösterildi. 3B TPU doku iskelelerindeki THP-1 makrofajların 3. günde CD68 boyaması 1, 7 ve 14. günlere kıyasla daha yoğundu. CD10 boyaması 1. günde 3, 7 ve 14. günlere kıyasla daha yoğundu. Sonuçlarımız, 3B TPU doku iskelelerinin makrofajlarla biyolojik olarak uyumlu olduğunu ve tıbbi uygulamalar için potansiyel bir biyomateryal olabileceğini göstermektedir.

Anahtar Kelimeler: makrofaj, 3D Baskı, TPU, Hücre Kültürü

Correspondence Address : Ufkay Karabay, Department of Molecular Medicine, Institute of Health Sciences Dokuz Eylul University, Izmir, Turkey ufkaykarabay@gmail.com

ORCID ID of the authors: M.Y.E 0000-0002-3570-1865 U.K 0000-0001-8608-1865, S.A 0000-0003-1263-9998, B.B 0000-0002-4178-2235 , R.B.H 0000-0003-1979-160X

Please cite this article in press at: Egrilmez M.Y., Karabay U., Aydemir S., Baykara B., Husemoglu R. B., The cellular responses of human macrophages seeded on 3D printed thermoplastic polyurethane scaffold, Journal of Medical Innovation and Technology, 2021; 3 (2):40-45 doi: 10.51934/jomit.1042774

1.Introduction

Tissue engineering is an interdisciplinary field of engineering and life sciences for the development of functional constructs that restore, maintain, or improve damaged tissues or whole organs (1). Substantial interest in three-dimensional (3D) printable biopolymers for applications, such as scaffolds in tissue engineering, drug delivery devices, as well as artificial organs for surgery trainings, are constantly growing.

3D-printed tissue engineering constructs are used to provide a biomimetic structural environment that facilitates tissue formation and promotes host tissue integration (2).

Thermoplastic polyurethanes (TPUs) are linear segmented block polymers containing polar hard segments and relatively nonpolar soft segments with crystalline and amorphous domains. This molecular architecture allows TPUs with an excellent stretchability and viscoelastic behavior (3). They are used in the field of medical applications particularly in flexible uses such as blood vessels, and catheters, as well as wound dressings. They are characterized by high biocompatibility, biodegradability, adequate bending strength and resistance to abrasion (4). Moreover, properly designed thermoplastic polyurethanes (TPUs) are suitable materials for use in 3D printing by the Fused Deposition Modeling (FDM) method [5].

The success of tissue engineering is strongly related to the inflammatory response. Implantation of biomaterials stimulates host responses aiming at eliminating the implants as foreign objects. Monocytes are crucial in this host inflammatory and foreign body reaction to biomaterials. An inflammatory response is initiated and monocytes migrate to the tissue–material interface (6). Once attached to the surface of the implant, they mature into a macrophage phenotype. Macrophages are key cells in the initial immune response to implants. They also regulate the recruitment, proliferation and differentiation of other types of cells including fibroblasts, endothelial cells, keratinocytes (7). They determine whether the inflammatory process subsides or a fibrous capsule forms and thus whether tissue regeneration occurs.

A profound understanding of how biomaterials control inflammatory response is important for the development of implants In particular, modulating the macrophage responses is of interest due to its relationship with not only the wound repair process, but also the foreign body response. The aim of this study is to investigate the viability, adhesion, distribution and CD68 and CD10 expression of human THP-1 macrophageses seeded on 3D printed TPU scaffolds in vitro.

2.Materials and Methods

Cell culture

The human monocytic leukemia cell line THP-1 was obtained from DSMZ (Germany). THP-1 cells were cultured using RPMI 1640 medium supplemented with 10% fetal bovine serum (FBS; Invitrogen), 2 mM L-glutamine, 100 U/ml penicillin and 100 µg/ml streptomycin at 37°C in a humidified 5% CO2 atmosphere. Cells were used for experiments between passage numbers 8 and 10. For differentiation to a macrophage phenotype, THP-1 cells were incubated with 100 nM of phorbol-12-myristate-13-acetate (PMA) (Applichem, Germany).

Fabrication of 3D Scaffolds

Scaffolds template (Ø = 4 mm, thickness = 2 mm) were designed using SolidWorks 2019 software and subsequently filled and sliced using and Ultimaker Cura 4.11 software to obtain cylindrical STL models. Briefly, clump generator software was used to create squared pores into a 3D object in a “stl” □le format. 3D-printed scaffolds were prepared from TPU (eSun Filament, Shenzhen, China). The 3D printer was a customized system working by the mechanism of FDM. Printing was performed by the custom made FDM printer, using a nozzle diameter of 0.4 mm, a layer thickness of 0.2 mm, a nozzle temperature of 240 °C TPU, and a printing bed temperature of 40°C. All scaffolds had a thickness of 2 mm. Both layers were printed with three perimeter lines and rectilinear filling under an angle of 0-90°, applying a flow rate of 100%. Printing speed was set to be 60 mm/s for all materials. Prior to biological evaluations, printed scaffolds were sterilized by ethylene oxide.

Cell Seeding on 3D Scaffolds

Sterile 3D TPU scaffolds were immersed in complete medium in the 96-well plate and incubated overnight in a humidified incubator (37°C, 5% CO2) prior to cell seeding. Then, suspension of THP-1 monocytes in complete medium with 100 nM PMA were seeded on the scaffolds at 4x104 cells per well and incubated in the same incubator for 4 h to allow cell attachment. Each well was completed to 150 µL complete medium in total volume. In order to eliminate the cells that do not attach to scaffolds, 16-24 hours after seeding the scaffolds were placed in another 96-well plate. THP-1 macrophages with equivalent numbers were also seeded on tissue culture plastic plates without scaffolds as a control group. 3D TPU scaffolds were cultured for 1 and 3 days.

Measurement of THP-1 macrophages viability on 3D TPU Scaffolds

The viability of THP-1 macrophages on 3D TPU scaffolds was determined by ready-to-use colorimetric WST-1 assay (Biovision, Milpitas, CA, USA) on days 1 and 3 after seeding of the cells. The assay protocol is based upon the cleavage of the tetrazolium salt WST-1 to formazan by cellular mitochondrial dehydrogenases. The amount of formazan dye produced was measured at 450 nm by using a microplate reader (Biotek Synergy HTX, USA). The cell viability was expressed in percentage relative to a control group.

Scanning electron microscopy

After seeding, THP-1 macrophages were cultured for 1 and 3 days on 3D TPU scaffolds. Then, they were fixed to evaluate the adhesion and the morphology of cells by scanning electron microscopy (SEM). The cell-scaffolds constructs were transferred to the 24-well plate, fixed in 4% paraformaldehyde, dehydrated through a graded series of ethanol solutions (60%, 70%, 80% and 99% ethanol) (v/v). Then the scaffolds were wrapped in aluminum foil and dried in the desiccator for 2 days (8). The scaffolds placed on the platform were plated with 5 nm gold for 20 minutes by the Q150R S (Quorum) instrument. Copper banding was then applied to the platform to eliminate charging effect. Images were taken by ZEISS Sigma 500 VP FE-SEM.

Histological staining of examination

THP-1 macrophages on 3D TPU scaffolds were cultured for 1, 3, 7, and 14 days. Cell-scaffold constructs were removed, washed three times in PBS and fixed in 4% paraformaldehyde at 4 °C for 24 h. This was followed by a tissue processing procedure, embedded in paraffin and cut into 5 µm thick sections. The sections were then stained with hematoxylin & eosin (H&E). The morphology and distribution of THP-1 macrophages cultured on 3D TPU scaffolds were examined under light microscope (Olympus, BX51 microscope) (9). In immunohistochemical (IHC) evaluation, 5 µm thick sections were treated with CD68 (bs-0649R, Bioss) and CD10 (bs-0709R, Bioss) antibodies and incubated at 4°C for overnight. Antigenic sites were visualized by diaminobenzidine solution and counterstained with hematoxylin. The images were taken with a light microscope (Olympus BX51 microscope) with X20 magnification (10, 11).

Statistical analysis

Statistical analyses were performed using SPSS 24 software program. The results were expressed as mean ± SD. Two groups were compared using Mann Whitney U test. A value of $p<0.05$ was considered significant.

3. Results

The viability of THP-1 macrophages on 3D TPU Scaffolds

Compared to the control cells seeded on tissue culture plastic plates without scaffolds, the number of THP-1 macrophages residing in the 3D TPU scaffolds showed a decrease on day 1 (p □ 0,05). The number of THP-1 macrophages on 3D TPU scaffolds showed the same trend on day 3 (p<0,05) (Figure 1).

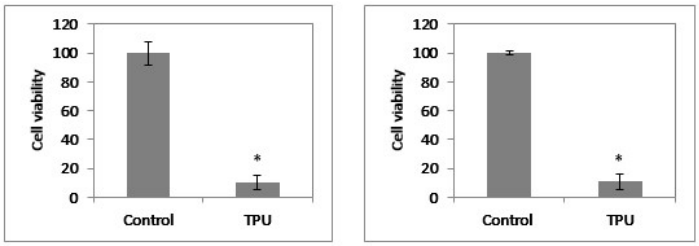

Figure 1. The viability of THP-1 macrophages on 3D TPU scaffolds on days 1 and 3.

The morphology of THP-1 macrophages on 3D TPU scaffolds

We investigated whether THP-1 macrophages were capable of adhering to 3D TPU scaffolds and vizualized via SEM. The cell distribution was homogeneous and THP-1 macrophages adhered to the surfaces of 3D TPU scaffolds on days 1 and 3. The cells were found to adhere to the scaffolds both in single cells and interacting cells. They showed a more rounded morphology on day 1 and a more elongated morphology on day 3 (Figure 2).

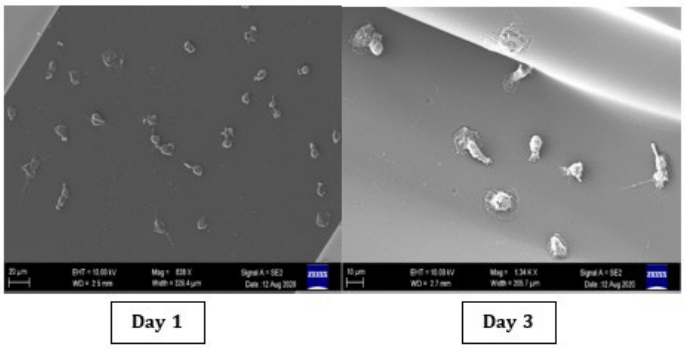

Figure 2. SEM images of THP-1 macrophages on 3D TPU scaffolds on days 1 and 3.

Histological analysis

THP-1 macrophages seeded on 3D TPU scaffolds showed tissue spesific morphologies in H&E staining on days 1, 3, 7, and 14. They were found to have eosinophilic cytoplasm and large nuclei. The distribution of cells on 3D TPU scaffolds were similar on all four days (Figure 3).

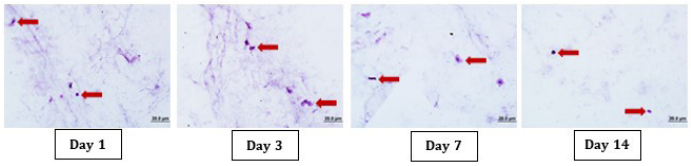

Figure 3. H&E staining in THP-1 macrophages seeded on 3D TPU scaffolds on days 1, 3, 7, and 14. Red arrows indicate THP-1 macrophages.

THP-1 macrophages on 3D TPU scaffolds were stained with CD68 (pan macrophage) macrophage marker to visualize the distribution of macrophages. Immunoreactivity for CD68 was observed in THP-1 macrophages on days 1, 3, 7, and 14. CD68 expression was stronger on day 3 compared to other days. THP-1 macrophages on 3D TPU scaffolds were also stained with CD10 antibody. CD10 expression was observed in THP-1 macrophages on days 1, 3, 7, and 14. CD10 expression was stronger on day 1 compared to other days.

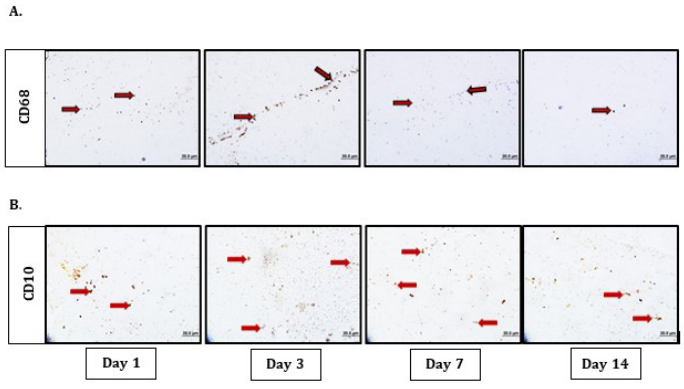

Figure 4. CD68 (A) and CD10 (B) staining in THP-1 macrophages seeded on 3D TPU scaffolds on days 1, 3, 7, and 14. Red arrows indicate CD68 (A) and CD10 (B) stained THP-1 macrophages.

4.Discussion

In our present study, we investigated the biocompatibility of 3D printed TPU scaffolds by using THP-1 monocyte-derived macrophages in vitro. THP-1 monocytes were treated with PMA and seeded on the 3D TPU scaffolds. Then, we analyzed the viability, adhesion. distribution and CD68 and CD10 expression of human THP-1 macrophages on the 3D TPU scaffolds.

Biomaterials are commonly used in medical applications. The application of 3D printing have greatly developed the manufacture of scaffolds in tissue engineering. TPU is a linear polymer that consists of hard and soft segments. They are used in medical applications, mainly because of its biocompatibility, high fracture strain, moderate tensile strength, and excellent abrasion and tear resistances. The soft segments provide elastomeric character, while hard segments usually provide additional strength (12).

The immune system is the first point of interaction between the body and the implant. It plays roles in biological processes required for the integration of biomaterials. Macrophages are instrumental in the host inflammatory and foreign body reaction to biomaterials. SEM images showed that THP-1 macrophages adhered to the surfaces of 3D printed TPU scaffolds on days 1 and 3 after seeding. This result showed the biocompatibility of 3D TPU scaffold with respect to THP-1 macrophages. The number of THP-1 macrophages on the 3D TPU scaffolds showed a decrease on days 1 and 3 compared to control group. We used 3D TPU scaffolds with soft properties in our study. A previous study showed that the number of 3T3 fibroblasts on soft TPU scaffolds were lower than hard TPU scaffolds (13). Woitschach et al reported that the number of human monocytes on soft TPU scaffolds were lower than hard TPU scaffolds (14). Our low cell viability results for TPU scaffolds are similar with these studies.

THP-1 macrophages seeded on 3D TPU scaffolds showed tissue spesific morphologies in H&E staining on days 1, 3, 7, and 14. They were found to have eosinophilic cytoplasm and large nuclei. CD68 is a pan macrophage marker (15). The presence of the macrophage CD68 positive THP-1 macrophages on 3D TPU scaffolds was evident on days 1, 3, 7, and 14. CD68 expression was stronger on day 3 compared to other days. CD10 is a cell surface neutral endopeptidase which is expressed by lymphocytes, neutrophils and monocytes (16). We observed CD10 expression in THP-1 macrophages on 3D TPU scaffolds on days 1, 3, 7, and 14. CD10 expression was stronger on day 1 compared to other days. A previous study showed that suspended THP-1 monocytes expressed no surface CD10 in the absence of PMA; however, after treatment with PMA, THP-1 cells differentiated to macrophages and CD10 was identified by flow cytometry (17). CD10 mRNA expression was also detected at 24 h and 72 h. Our result in consistence with this study

showed CD10 expression in THP-1 macrophages on 3D TPU scaffolds. Our histological observations demonstrated the presence and distribution of THP-1 macrophages on 3D TPU scaffolds.

5. Conclusion

In the present study, 3D printed TPU scaffolds was evaluated for the cellular responses of THP-1 macrophages in vitro. Our results provide data to better understand the immune responses and immunoengineering strategies using macrophages.

References

1. Langer R, Vacanti JP. Tissue engineering. Science. 1993;260:920-6.

2. Richards DJ, Tan Y, Jia J, Yao H, Mei Y. 3D Printing for tissue engineering. Isr J Chem. 2013;53:805-14.

3. Harynska A, Kucinska-Lipka J, Sulowska A, Gubanska I, Kostrzewa M, Janik H. Medical-Grade PCL based polyurethane system for FDM 3D Printing-Characterization and Fabrication. Materials (Basel). 2019 Mar 16;12:887.

4. Joseph J, Patel RM, Wenham A, Smith JR. Biomedical applications of polyurethane materials and coatings. Trans Inst Met Finish. 2018;96:121-29.

5. Xiao J, Gao Y. The manufacture of 3D printing of medical grade TPU. Prog Addit Manuf 2017; 2: 117-123.

6. Anderson JM. Biological responses to materials. Annu Rev Mater Res 2001; 3: 81-110.

7. Martin KE, García AJ. Macrophage phenotypes in tissue repair and the foreign body response: Implications for biomaterial-based regenerative medicine strategies. Acta Biomaterialia 2021;133:4-16.

8. Farrugia BL, Brown TD, Upton Z, Hutmacher DW, Dalton PD, Dargaville TR. Dermal fibroblast infiltration of poly(ε-caprolactone) scaffolds fabricated by melt electrospinning in a direct writing mode. Biofabrication. 2013;5: 025001.

9. Huerta RR, Silva E, Ekaette I, El-Bialy T, Saldaña MDA. High-Intensity ultrasound-assisted formation of cellulose nanofiber scaffold with low and high lignin content and their cytocompatibility with gingival fibroblast cells. Ultrason Sonochem 2020;64:104759.

10. Chen WC, Wei YH, Chu IM, Yao CL. Effect of chondroitin sulphate C on the in vitro and in vivo chondrogenesis of mesenchymal stem cells in crosslinked type II collagen scaffolds. J Tissue Eng Regen Med 2013;7:665-72.

11. Griffin MF, Naderi N, Kalaskar DM, Seifalian AM, Butler PE. Argon plasma surface modification promotes the therapeutic angiogenesis and tissue formation of tissue-engineered scaffolds in vivo by adipose-derived stem cells. Stem Cell Res Ther 2019;10:1-14.

12. Tatai L, Moore TG, Adhikari R, Malherbe F, Jayasekara R, Griffiths I, Gunatillake PA. Thermoplastic biodegradable polyurethanes: The effect of chain extender structure on properties and in-vitro degradation. Biomaterials 2007;28:5407-17.

13. Mi HY, Jing X, Salick MR, Cordie TM, Peng XF, Turng LSh. Properties and fibroblast cellular response of soft and hard thermoplastic polyurethane electrospun nanofibrous scaffolds. J Biomed Mater Res B Appl Biomater . 2015;103:960-70.

14. Woitschach F, Kloss M, Schlodder K, Borck A, Grabow N, Reisinger EC, Sombetzki M. In vitro study of the interaction of innate immune cells with liquid silicone rubber coated with zwitterionic methyl methacrylate and thermoplastic polyurethanes. Materials 2021;14:5972.

15. Gordon S, Plüddemann A, Martinez Estrada F. Macrophage heterogeneity in tissues: phenotypic diversity and functions. Immunol Rev 2014;262:36–55. Erdos EG, Skidgel RA. Neutral endopeptidase 24.11 (enkephalinase) and related regulators of peptide hormones. FASEB Journal 1989;3:145-151.

16. Huang X, He C, Lin G, Lu L, Xing K, Hua X, Sun S, Mao Y, Song Y, Wang J, Li S. Induced CD10 expression during monocyte-to-macrophage differentiation identifies a unique subset of macrophages in pancreatic ductal adenocarcinoma, Biochem Biophys 2020;524:1064-71.

Review

Four-Dimensional Printing Technology at the Frontier of Advanced Modeling and Applications in Brain Tissue Engineering

Gelişmiş Modellemede Yeni Alan Dört Boyutlu Baskı Teknolojisi ve Beyin Doku Mühendisliğinde Uygulamaları

Merve Nur Soykan[1,2], Tayfun Şengel[2,4], Aliakbar Ebrahimi[1,5], Murat Kaya[1], Burcugül Altuğ-Tasa[1], Hamed Ghorbanpoor[1,3], Onur Uysal[1,2], Ayla Eker Sarıboyacı[1,2], Hüseyin Avcı[1,2,5,6]

1 Cellular Therapy and Stem Cell Production Application and Research Centre, ESTEM, Eskisehir Osmangazi University, Eskisehir, Turkey

2 Department of Stem Cell, Institute of Health Sciences, Eskisehir Osmangazi University, Eskisehir, Turkey

3 Department of Biomedical Engineering, Eskişehir Osmangazi University, Eskişehir, Turkey

4 Central Research Laboratory Research and Application Center, Eskisehir Osmangazi University, Eskisehir, Turkey

5 Department of Metallurgical and Materials Engineering, Eskişehir Osmangazi University, Eskişehir, Turkey

6 Translational Medicine Research and Clinical Center, Eskisehir Osmangazi University, Eskisehir, Turkey

Abstract: The complex process behind the brain topology, which has been extensively studied for the last ten years, is still unclear. Therefore, neural tissue engineering studies are needed to better understand cortical folds. With the development of 4-dimensional (4D) bioprinters using cell-loaded smart materials, a promising path has been opened in the mimicry of the neural tissue. In our study, we review the usage areas of 4D printers, which have been developing in recent years, in modelling brain tissue. As a result of development of smart materials printed with 3-dimensional (3D) printers caused emerging of 4D printers, rapidly. Smart materials can change their properties based on physical, chemical and biological stimuli, and this change can be a reversible process. Cell-loaded printed smart materials should have little effect on cell viability of both the incoming stimulus and the physical change. It is also important that the material used is non-toxic and the solvent is suitable for cell viability. On the other hand, hydrogels are frequently studied to mimic the complex neural network of neural tissue. Agents that affect the crosslinking or degree of crosslinking of hydrogels can be easily controlled and changed. In addition, studies with neural stem cells have shown that hydrogels have a supportive effect on the proliferation and maturation of neural stem cells. Since the folding time, strength and location of smart materials cannot be known precisely, it can be an advantage of 4D bioprinters as it can be controlled and studied whether the results of the stress on the cells in this region will affect other cells. It is an ideal methodology to study the effect of cortical folding on neural stem cells, especially thanks to the ease of experimental manipulations provided by 4D bioprinters. It is expected that 4D bioprinters will be adopted and rapid developments will occur in the multidisciplinary field of tissue engineering of brain tissue in the near coming years.
Keywords: Neural-tissue engineering, Neural modeling, 4D Printer, Smart biomaterial, Shape memory

Özet: Son on yıldır kapsamlı çalışmalar yapılan beyin topolojisinin arkasında yatan süreç henüz belirsizdir. Kortikal katlanmaların daha iyi anlaşılabilmesi için nöral doku mühendisliği çalışmalarına ihtiyaç vardır. Hücre yüklü akıllı malzemelerin kullanıldığı 4 boyutlu (4B) biyoyazıcıların gelişmesi ile nöral dokunun mimik edilmesinde umut verici bir yol açılmıştır. Çalışmamızda son yıllarda gelişmekte olan 4B yazıcıların beyin dokusunun modellenmesinde kullanım alanlarını gözden geçirmekteyiz. 3 boyutlu (3B) yazıcılar ile basılan akıllı malzemelerin gelişmesiyle 4B yazıcılar ortaya çıkmıştır. Akıllı malzemeler fiziksel, kimyasal ve biyolojik uyaranlara dayalı olarak özelliklerini değiştirebilirler ve bu değişiklik geri dönüşümlü bir süreçtir. Hücre yüklü olarak basılan akıllı malzemeler hem gelen uyarıcının hem de fiziksel değişimin hücre canlılığı üzerinde çok az bir etki yaratması gerekir. Ayrıca kullanılan malzemenin toksik olmaması ve çözücünü hücre canlılığına uygun olması da önemlidir. Nöral dokunun karmaşık sinir ağının mimik edilebilmesi için hidrojeller ile sıklıkla çalışılmaktadır. Hidrojellerin çapraz bağlanmasını veya çapraz bağlanma derecesini etkileyen ajanlar kolaylıkla kontrol edilebilir ve değiştirilebilir. Ayrıca nöral kök hücreler ile yapılan çalışmalarda hidrojellerin nöral kök hücrelerin proliferasyon ve olgunlaşması üzerinde destekleyici bir etkiye sahip olduğu gösterilmiştir. Akıllı malzemelerin katlanma zamanı, kuvveti ve yeri kesin olarak bilinemediği için bu bölgede bulunan hücreler üzerindeki stresin sonuçlarının diğer hücreleri etkileyip etkilemeyeceğinin ön görülmesi zorluğu 4B biyoyazıcıların bir avantajı olarak karşımıza çıkma ihtimalini göstermektedir. Burada özellikle 4B biyoyazıcıların sağladığı deneysel manipülasyonların kolaylığı sayesinde kortikal katlanmanın nöral kök hücreler üzerine etkisini incelemek için ideal bir metodolojidir. Önümüzdeki yakın yıllarda multidisipliner olan beyin doku mühendisliği alanında 4B biyoyazıcıların benimseneceği ve hızlı gelişmelerin olacağını düşünmekteyiz.
Anahtar Kelimeler: Nöral doku mühendisliği, Nöral modelleme, 4B yazıcı, Akıllı biyomalzeme, Şekil hafızası

Correspondence Address : Merve Nur SOYKAN Cellular Therapy and Stem Cell Production Application and Research Centre, ESTEM, Eskisehir Osmangazi University, Eskisehir, Turkey mervesykn@gmail.com

ORCID ID of the authors: M.N.S. 0000-0003-1231-9791, T.Ş. 0000-0002-1162-6979, A.E. 0000-0001-6437-7796, M.K. 0000-0002-4277-6304, B.A.T. 0000-0003-4460-8467, H.G. 0000-0002-2665-8172, O.U. 0000-0001-6800-5607, A.E.S 0000-0003-4536-9859, H.A. 0000-0002-2475-1963

Please cite this article in press at: Soykan M.N., Şengel T., Ebrahimi A., Kaya M., Tasa B.A., Ghorbanpoor H., Uysal O., Sarıboyacı A.E., Hüseyin Avcı H., Four-Dimensional Printing Technology at the Frontier of Advanced Modeling and Applications in Brain Tissue Engineering, Journal of Medical Innovation and Technology, 2021; 3 (2):46-57 doi: 10.51934/jomit.1016838

1.Introduction

The human brain is an organ with a more complex structure compared to other organs in the body. Today, there is still insufficient information about brain development and diseases. Studies with animals for brain studies are limited due to differences in the structure of the animal and human brains. Therefore, human brain-like structures are needed to investigate unknown processes [1]. The topology of brain tissue has been the subject of extensive studies for the last ten years, but the process behind the formation of this topology is still unclear [2]. The folds of the cerebral cortex, called gyri and sulci, are one of the most distinctive features of the mammalian brain. It was believed that during evolution there was a milestone in the formation of cortical folds, which allowed an increase in the number of neurons in the cerebral cortex. An increase in the number of neural progenitors is thought to be responsible for cortical folding [3]. The folding structure of cortical tissues is effective on neurological development of schizophrenia, autism etc. It is known that abnormal cortical folding is responsible for psychotic disorders [4]. In order to better understand the cortical folding, the existing theoretical models have been studied with various materials. However, due to the absence of living cells in these studies, the physiological parameters that closely affect tissue development such as folding and hardening of the material is hard to explain [5].

Neural tissue, which has a cytologically heterogeneous structure, differs mechanically in certain regions due to this heterogeneity. The distribution of cell types in cortical and subcortical tissue, cell migration and proliferation affect the mechanical properties of the tissue and play a role in the folding process. Tissue folding signal starts via cells. The neurological function of normal or abnormal folding is a result of many processes that affect folding. It is essential for neurological diseases to mimic the cortical tissue folding process in a biologically correct and appropriate way during the neural development process.

Neural models have special requirements. These can be neurocompatibility to allow nerve cells to attach and proliferate, elastic properties to mimic the mechanical and physicochemical properties of natural nervous tissue ECM, hierarchical microarchitecture and the ability to induce electroconductivity. The use of cell-loaded smart materials has the advantage of mimicking the mechanical tension associated with cortical folding and imparting neural cell maturation and functionality. In addition to these advantages, the fact that the biomechanical properties can be adjusted and changed in the examination of the folding structure of neurological diseases also allows the creation of the most physiologically correct model [6]. Recent advances in four-dimensional (4D) bioprinters have opened up a promising way to mimic living neural tissue [2]. Due to the wide variety in the field, it would be impossible to cover every facet of subject comprehensively. Therefore, the objective of this review paper is to provide a critical and constructive analysis of the recent literature with a particular focus on development of the technology and their application in neural-tissue engineering.

2. 4-Dimensional (4D) Bioprinter

Three-dimensional (3D) printing, known as additive manufacturing, is very popular nowadays. Due to the fact that complex objects are produced with high accuracy and with much less waste material, this technique has found numerous practical applications in the automotive, aerospace, energy and other fields [7,8]. With the development of 3D-printed structures on the basis of captured tissue photos with medical imaging systems such as computed tomography (CT) and magnetic resonance imaging (MRI), due to the need for high structural complexity and design flexibility for patient-specific surgical models and prostheses should be easily manufactured. One of the advanced additive manufacturing studies is 3D bioprinting, which contributes to the production of tissue-like structures [9-12].

The term 3D bioprinting is used to refer to the layer-by-layer positioning of biological materials, biochemical and living cells to create bioengineered structures that mimic natural living systems. This technology plays a role in ensuring proper spatial and temporal control over cell location, especially in regenerative medicine. As a result, the need for donor organs can be eliminated and the risk of tissue rejection can be reduced However, the sensitivity of living cells, cell types, growth/differentiation factors and material selections in 3D bioprinting are quite complex compared to conventional 3D printing. At the same time, there is a need to develop technical strategies for obtaining living cells and generating 3D structures with appropriate properties for the proper functioning of tissues or organs [13-15].

On the other hand, there may be some limitations in the widespread use of 3D bioprinting. This is because, while native tissues constantly change their morphology to stimuli in their environment, ordinary 3D bioprinted structures cannot elicit appropriate biological responses in their microenvironment. Recently, a new concept called four-dimensional (4D) bioprinting has begun to help alleviate this problem. In this method for fabricating biologically active structures that can adjust their properties to one or more stimuli to achieve the required functionality, the dynamics of natural tissues can be more precisely mimicked when stimuli-sensitive materials are integrated with 3D bioprinting [16-18].

4D bioprinting offers very important innovations and advantages under current conditions for productions that cannot be obtained with other biofabrication method such as 3D printing / bioprinting in order to solve the needs for high resolution dynamic structures. One of the important advantages of 4D bioprinting is it enables the creation of arbitrary controllable shapes by integrating the time dimension as an additional dimension to the 3 spatial dimensions (x, y, z) of the object [19, 20].

Chadwick et al. fabricated 4D cell culture arrays with a temperature-sensitive and shape-memory polymer that can be deformed into a non-permanent deformation and revert to its pre-deformation state when heat-treated to rapidly assess drug responses of glioblastoma patient-derived models. These arrays can spontaneously transform from 3D cell culture inserts into histological cassettes over time when heated [21].

Smart materials have a "shape-changing effect (SCE)" due to both their properties and the change of shape of the material or its return to its original state depending on external stimuli. With the SCE feature, the first intelligent material was developed at the Massachusetts Institute of Technology (MIT) [65]. Materials with SCE properties are not homogeneous, on the other hand, they need a stimulus such as light, temperature, humidity, or pH in order for the shape-changing property to be activated. As the details of the shape changes of intelligent materials in response to stimuli are understood, many types of intelligent materials have been developed and used in practice for the production of precisely programmed 4D bioprints [12, 19].

The 4D printer actually gains another dimension by changing shape due to a stimulus, which is obtained by using smart materials in 3D printers. The new dimension to be gained in the product of the 3D printer is predictable as a result of precise programming. If the material cannot return to its original state after the effect of the stimulus has passed, it is called unidirectional, if it can return, it is called double or multi-directional smart material [13]. After printing on both 3D and 4D printers (cell scaffolding) or if there are cells inside the printed material (bioink), these printers are called bioprinters. In 4D bioprints, both the incoming stimulus and the physical change should have very little effect on cell viability. In addition, it is ideal that the material is not toxic to the cell and its solvent is cell culture medium, PBS or water [2].

3. 4D Bioprinting Based On Shape-Transformation Mechanism

Stimuli-responsive materials or smart materials can change their properties based on physical, chemical and biological stimuli. Physical stimuli (humidity, photo, temperature, acoustic, electro, magnetic), biological stimuli (glucose and enzymes) and chemical stimuli (pH, ions) materials have the potential to play as an on-off switch system in different areas. These stimuli changes as a response for environmental conditions are reversible process and can be repeated at the same conditions for several times [22]. By changing in structural properties of 3D printed materials as function of time, the capacity and ability of 3D printed materials increase and the fourth dimension was added to system therefore 4D printing concept have been found [23]. Among the different stimuli, water (humidity) was the first stimuli used in 4D bioprinting. When water-sensitive materials exposed to surrounding environment, they can absorb or release moistures, and as a results swelling, twisting, folding and other deformations can be stimulated [24].

3.1. Physical Stimulations

Physical stimuli such as temperature, liquid/humidity, light, magnetic field, and electrical stimulation have generally caused structural and shape changes in materials sensitive to stimuli, enabling us to obtain materials with unique properties and have led to the use of very different areas in application areas. Using polymers that exhibit different swelling/shrinking behaviors with temperature used as a physical stimulus have been carried out [25, 26]. Zarek et al. (2017) produced a methacrylate polycaprolactone-based stent in their study. This stent expanded with temperature and developed a stent that fully adapts to this section [27]. In this way, it can be ensured that no injury occurs during the stent placement process and can be expanded and fully conformed afterward. Stoychev et al. (2011) [28] obtained a double-layered polymer using polycaprolactam and poly-(N-isopropyl acrylamide) in their study. While this polymer is in star form at 60°C, it takes a folded shape at 25°C -33°C. Apsite et al. (2017) [29] created different bilayer and trilayer structures with electrospinning in their study using PCL and NIPAM. In two-layer films, the fiber structure is designed in parallel direction. While there was no folding in the obtained films at room temperature and dry, different foldings were detected when wet at 20°C and 37°C. The bilayer films are shown to be folded around the long direction with respect to the orientation of the fiber structure when wet and at 20°C. Wet and 37°C both bilayer and trilayer films showed folding around the short direction (Fig. 1).

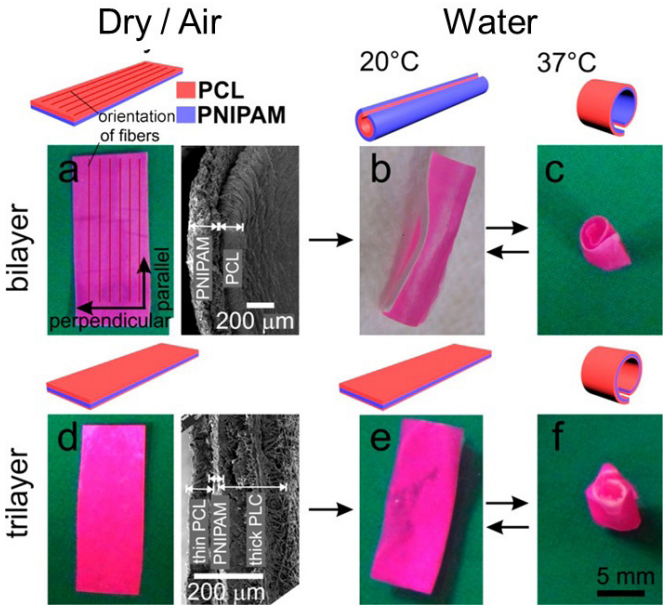

Figure 1. p(NIPAM-BPA)-PCL bilayer and PCL-p(NIPAM-BPA)-PCL trilayer electrospun mats: (a) and (d) left, bilayer and trilayer mats no folding is air at room temperature, (b) long-side rolling for bilayer mats (water, 20 °C), (c) short-side rolling for bilayer mats (water, 37 °C), (e) no folding trilayer mats (water, 20 °C), (f) short-side rolling for trilayer mats (water, 37 °C). Reprinted with permission from [29]. Copyright 2017 American Chemical Society

Another physical factor is liquid/moisture. Humidity is the trigger of some known phenomena in nature. For example, pinecones open under low humidity conditions and release seeds into the environment. Natural events like this have inspired materials that change shape and size with moisture [30]. Cell encapsulation in smart materials is used for controlled drug release or valve-like smart studies with swelling/shrinking. However, these materials have slow response times, poor mechanical properties, and decomposition/hydrolysis properties are important considerations [16,31].

The study of light as a physical stimulus in polymers has led to the development of photosensitive biomedical devices. Size and shape changes, charge formation, photodimerization, and zwitterionic species formation can be induced by light [16]. Gupta et al. (2015) [32] obtained capsules loaded with gold nanorod, PLGA, and therapeutic molecules using a 3D printer (Fig. 2). When these materials were excited with a laser, fragmentation in the shell portion followed by the release of therapeutic molecules was achieved.

Electrosensitive or conductive materials is another physical factor that has come to the fore in recent years, especially because it provides cellular tropism and has positive effects on tissue regeneration [33, 34]. These materials are polymers that exhibit swelling shrinkage behavior or fold under an external electric field. As electrically steerable materials, this type of perspective can be considered in drug release or repair/regeneration models. Graphene and carbon nanotubes, which have attracted much attention in recent years and inspired studies with high conductivity, can add durability and electrical conductivity properties to biomaterials. Especially considering conductivity, studies in nerve tissue engineering using 3D and 4D bioprinting techniques are promising. Sayyar et al. (2016) and Janus et al. (2015) obtained tissue scaffolds containing various amounts of graphene in their study. These studies with scaffolds have shown that while cellular viability is not affected, they support the differentiation of mesenchymal stem cells due to the application of electricity [35, 36].

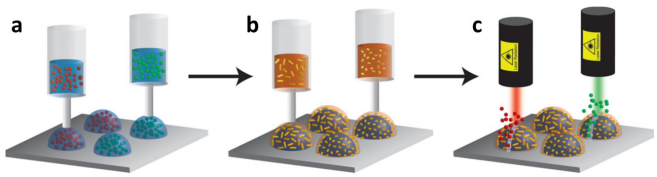

Figure 2. Programmable printing and rupturing of capsules: (a) the core containing biomolecules is printed directly onto a substrate with a 3d printer; (b) PLGA solutions containing gold nanorods are dispensed directly onto the nuclei, resulting in a stimulus-sensitive shell.; (c) The capsules are selectively disintegrated by irradiation with a laser beam. Reprinted with permission from Gupta vd;2017. Copyright 2017 American Chemical Society

3.2. Chemical Stimulation

There are two main chemical stimuli materials. pH responsive materials [37] and ion sensitive hydrogels. pH responsive materials have weakly acidic [38, 39] or weakly basic [40] functional groups like carboxyl, sulfonic, phosphate, and pyridine [16]. At high pH, polymers with weak acidic functional groups (polyacids) release protons to become negatively charged. Polymer chains are approximately very close to each other and as a result the parts of the polymer chains with same charge repulse each other. The same procedure take place for polymers with weak basic functional groups (polybases) as a results of protonation in low pH. Some polymers (collagen, gelatin, and keratin, chitosan, hyaluronic acid, and dextran) are responsive to the environmental pH

value. By change in pH, these chemical groups can release or accept protons and swelling or collapsing accrued as result of protonation and deprotonation. These properties can be applied for designing of self-assembled structures [16, 37, 41].

Ramos et al. offered a low cast strategy for preparing keratin hydrogel that have enhanced mechanical properties. Obtained hydrogel have enough stiffness to handle without any specific cares and also present reversible pH-responsive character. At low pH minimum amount of swelling was reported as a result of collapsing of protein network and water molecules tightly adsorbed to the hydrophilic areas inside the hydrogel. By increasing the pH (above the pH 6), swelling ratio rises sharply and the maximum amount of swelling was reported at pH above 8 where the expanded network of hydrogel allows water to enter inside the pores [42].

Narupai et al. used protein based material for preparing 3D printed hydrogels and applied them for structural changes (temperature, pH, or an enzyme) that can be controlled and reversible. Methacrylated bovine serum albumin (MA–BSA) with biodegradable character used to Pickering emulsion gels. Hydrogel formation process take place in presence of N-isopropylacrylamide or 2-dimethylaminoethyl methacrylate. Synthesized hydrogels are ideal material for 3D printing of multi-layer stimuli-responsive objects. Poly(N-isopropylacrylamide) P(NIPAAm) and poly(dimethylaminoethyl methacrylate) (P(DMAEMA)) add temperature (T) and pH-responsive character into the obtained hydrogels. Also enzyme-triggered shape change can occur because of the degradation of the BSA network. These hydrogels can reversibly change shape due to by change in temperature or pH, and also enzymatic degradation can occur in irreversible manner and these complex changes could be added to 4D printed systems (Fig. 3) [43].

Another group of chemical stimuli responsive materials are ion-sensitive materials. These materials have the sensitivity to ionic concentration of the surrounding environment [22, 24, 44]. Some of ion sensitive materials, especially ion-sensitive hydrogels, have capability of introducing to 4D bioprinting systems. In these materials, crosslinking and dissociation between the polymer chains as a result of interacting with ions is the base of their ion-sensitive behavior [45]. Like pH responsive materials, in ion-responsive hydrogels the polymer chains are mainly linked through electrostatic interactions, decrease or increase of the ion concentration can change the strength of the electrostatic interaction and effect the behavior of the hydrogels.

Alginates as an ion-senstive gels is a case in point. Alginates have ability to create ion-senstive gels by electrostatic crosslinking. So they have potential for creating in situ gellable materials in presence of divalent cationic environments such as Ca2+ [45].

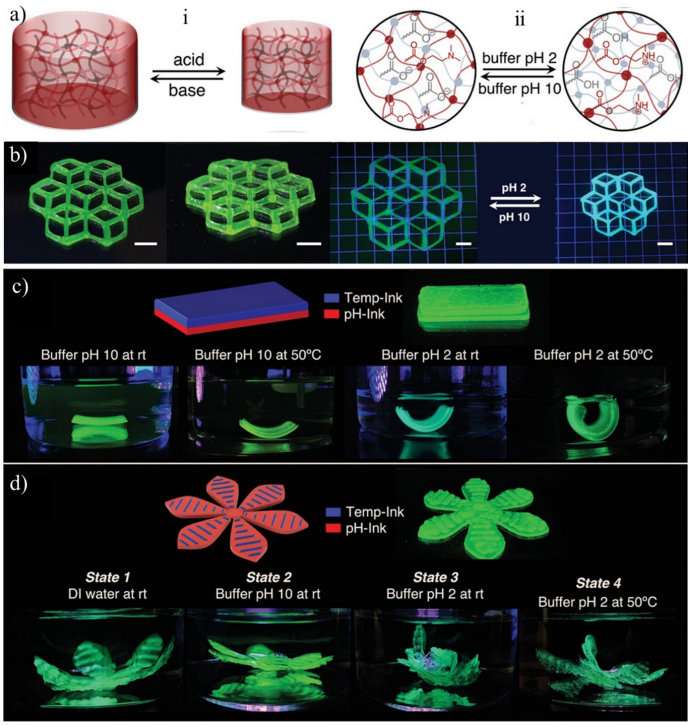

Figure 3. a) i. after photopolymerization, the pH-sensitive hydrogel shrinks reversibly when immersed in acidic solution and expanded when immersed in basic solution, ii. Chemical composition of the pH responsive hydrogel: amine (P(DMAEMA)) and carboxylic acid (MA--BSA) groups. b) 3D printed structure and pH response of the hydrogel. c and d) Multiple shape transformations of 3D printed hydrogel structures. c) pH and temperature-responsive bilayer. d) Complex flower morphology using pH-Ink for petals and Temp-Ink for lines across each petal. Reprinted with permission from [43] Copyright (2021) John Wiley and Sons.

Wang et al. reported design and synthesize of fluorochromic hydrogels that are sensitive to light and ferric ion (Fe3+) [47]. These hydrogels have high strength and self-healing ability. Poly(vinyl alcohol) (PVA) physically cross-linked in the presence of tannic acid and γ-cyclodextrin-spiropyran (γ-CD-SP) and PVA based hydrogel were synthesized. Formation of Hydrogen bonds between the PVA chain and γ-CD moiety, allow the fluorophore γ-CD-SP addition inside the PVA gel. The hydrogel have "on/off" fluorescence property due to photo-isomerization character of the SP moiety. The fluorescence emission property of hydrogel can be turned off by adding Fe3+ as result of fluorescence inner filter effects, and the process can be recovered by adding EDTA. These properties (high strength, self-healing,

and tunable fluorescence) make the hydrogels capable materials for use in optical switches, wearable devices, and fluorescent sensors.

3.3. Biological Stimulation

There is always a signal-response system in the human body. For example, blood sugar is constantly regulated by insulin secretion. In today's studies, studies aimed at gaining sensitive behavior when interacting with free-form materials gain importance [16].

Glucose is the most frequently found free biochemical in the blood and is the most important marker of diabetes; the diagnosis and follow-up are the most difficult. Glucose-sensitive polymers respond to changes in glucose concentration and are promising in targeted diabetes treatment applications. As diabetes becomes one of the social health problems, interest in a glucose-sensitive polymer is increasing. The change in glucose concentration causes a change in the properties of the polymer [48].

Considering the studies, there are studies on determining the glucose level by amperometric method from conductive polymeric structures modified with glucose dehydrogenase or glucose oxidase. In these studies, the detection range was 0 – 400 mg/dL [49]. Both the monitoring of blood glucose levels and the timely use of regulatory drugs are essential for the prognosis of diabetes. While innovative technologies are used in sensors to monitor blood levels, studies have recently been conducted on releasing insulin from the polymer depending on the glucose level in drug delivery systems. In these studies, insulin release occurs either due to polymeric hydrolysis after the interaction of glucose oxidase with glucose or due to the binding of glucose in the polymeric membrane structure of insulin [50, 51]. Enzymes such as glucose are free materials in the blood or body. Enzymes are important compounds that catalyze various reactions in the human body and are involved in particular reactions. The ability of enzymes to cleave specific bonds in the engineered natural or synthetic polymer is a critical approach. Enzyme-sensitive polymers have a significant advantage in drug delivery due to their self-occurrence in the biological environment. However, there are important issues such as the polymers to be designed do not react with other enzymes, be biocompatible, non-toxic, and release active compounds such as drugs in the target tissue [52].

At the beginning of these studies is drug retention in polymeric structure or side chains and its degradation by enzyme release. In this way, it is possible to develop materials that can be tissue or disease-specific applications [53]. Apart from these, soft robotic approaches that have come to the fore recently are based on structures produced from enzymatically degradable materials. These tiny devices have shown great potential in targeted drug delivery, microsurgery, and detection and diagnosis. A significant challenge in small-scale biomedical robotics is to design functional micro and nanostructures that can perform multiple tasks and be implanted in the body (Fig. 4) [54]. Current trends in micro and nanorobots are towards adopting soft materials that are more suitable for biomedical applications because their physicochemical properties are more similar to those of tissues [53, 54].

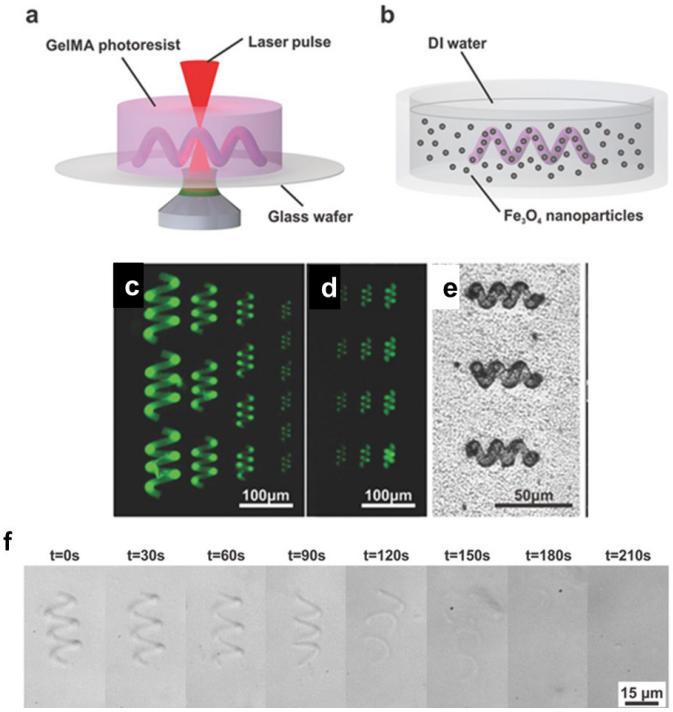

Figure 4. Biodegradable GelMA helical microswimmers: a) Photoresist is used to print GelMA helical structures; and b) decorated with magnetic nanoparticles; c) and d) fluorescent microscope images of helical structures of different sizes and thicknesses. e) Optical image of helical microswimmers decorated with magnetic nanoparticles. f) Time-dependent degradation of helical structures in collagenase solution(0.1 mg mL^{-1}). Reprinted with permission from [54]. Copyright 2018 WILEY-VCH Verlag GmbH & Co. KGaA, Weinheim.

4. Applications of 4D Printing in Neural-Tissue Engineering

The materials, which can best mimic the complex nerve structure in the tissue can be hydrogels. Because the agents that affect the crosslinking of hydrogels or the degree of crosslinking can be easily controlled and changed with adding a various supportive materials. In

addition, studies have found that it has an encouraging effect on the proliferation and maturation of neural stem cells [55]. However, since the precise time, force and location of folding in smart materials used in 4D bioprinters are not controlled, it is not known which consequences of the stress will be on the cells in the region of folding. In 4D prints with hydrogel material, it has been shown that cells can move to the upper and lower points where they form the folds [56].

The current literature on 4D bioprinting of nerve tissues is very limited. Some of the studies using 3D and 4D bioprinters are compared and shown in Table 1. A brief summary of the literature has been investigated to describe the advantages and deficiencies in 3D bioprinting studies while moving towards 4D models. Lozano et al. produced a six-layer cerebral cortex model. For their study, the new RGD-peptide-modified Gellan Gum (GG) bioink was developed to encapsulate primary cortical neurons which modeled from mouse embryos. Cells encapsulated with a bioink 5X DMEM and 1M calcium chloride which can be cross-linked without toxic effects. In this study, it was determined that the encapsulated cells continued to grow, divide and form neural networks during the 5-day culture period, and occurred axonal development from the cell-loaded layers to the empty layers [57]. In another study, the viability and proliferation of cells were evaluated in order to form tissue grafts for regenerative medicine with inject printing technology using retinal ganglion and glia cells, which are cells of the adult rat central nervous system [58].

The structure and development of neural tissue have significant role when mimicking the folding process of cortical tissue with 4D bioprinters. For instance, it must be similar to the tissue network of gray and white matter in vivo for biomimicking neural tissue. Considering this situation, 4D printing are carried with brain gray matter modulus 0.68 ± 0.20 kPa, cerebral white matter modulus 1.41 ± 0.66 kPa, and cerebellum modulus 0.75 ± 0.29 kPa [2]. Moreover, biomimicry of neural tissue must have a folding rate similar to in vivo in order to mimic the folding of cortical tissue. In other words, in order to biomimic the cortical tissue, it is necessary to model it to fold or form a flat structure for 10 or more weeks in in vitro conditions. Heat-sensitive shape memory polymers (SMPs) can be used to mimic neural tissue. They are thermosetting polymeric compounds that are easy to modify, but the shape given by heat is permanent [59]. However, in recent studies, SMPs varieties have been applied that can be folded 180° by changing the formulation of SMP polymers and can be restored at 37°C. For example, soybean oil epoxidized acrylate can recover its former structures at 37°C (Fig. 5a) [60]. Miao et al., successfully produced a 4D-printed graphene-enabled polymeric nerve routing channel that can be used for directing guidance of stem cell growth (Fig. 5b-5d). They produced it for regeneration of the peripheral nervous system using custom-made stereolithography. Human bone marrow mesenchymal stem cells (hMSCs) were demonstrated to sequence in an aligned manner on scaffolds created using a 4D printer. It was shown that the 4D-printed scaffold improved expression of neurogenic factors ND1, NSE and Ngn2 in comparison of control samples. Moreover, the spatial features required for neural development safely increased neurogenesis. In this study, naturally derived memory polymer 4D effect is suitable for thermomechanical programming [61].

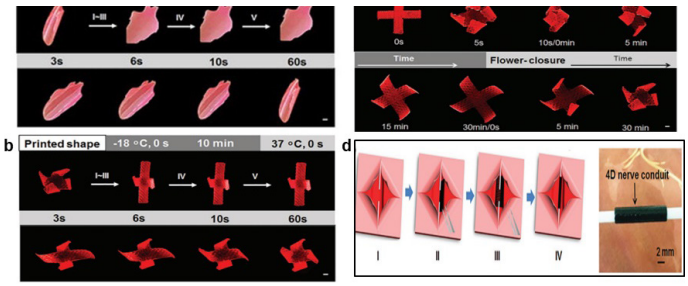

Figure 5. a and b) SOEA-based materals that can temporarily take a flat shape at -18°C and fully recover their original shape at 37°C . (Reprinted with permissions from [60] Copyright (2019) Taylor & Francis Online and [60] Copyright (2018) John Wiley and Sons). c) Photographs of the reversible shape process with a 4D-printed flower structure that can be opened in ethanol and closed in water. (Reprinted with permission from [60] Copyright (2018) John Wiley and Sons). d) 4D nerve guidance conduit, Schematic of the self-entubulation in a damaged nerve (I-IV). (Scale bar, 2 mm). (Reprinted with permission from [61] Copyright (2018) John Wiley and Sons).

Table 1. Summary of recent researches on 3D and 4D printing for neural-tissue engineering.

Approach	3D Printing	4D Printing
Materials	Gellan gum-RGD (RGD-GG) [57] CNS grafts [58] 10% GelMA and 15% PEGDA [63] S 4-arm PLA [64]	SOEA [61] AlgGel [62]
Printing Technique	Harpool Luer-lock syringes [57] Piezoelectric inkjet printing [58] Stereolithography-based 3D printer [63] A direct laser write (DLW) [64]	Stereolithographic [61] XY-axis positioning system [62]
Stimulus		Ethanol [61] Calcium-free PBS [62]
Advantages	Opportunity to provide a more accurate representation of 3D in vivo environments with applications ranging from cell behavior studies [57] Opening new avenues for printed CNS grafts in regenerative medicine [58] 3D printing technology is superior to many other conventional scaffold fabrication approaches regarding the design and controllability of architecture [63] Good mechanical properties [64]	Creating multiresponsive smart architectures [61] 4D-printing platform suitable for engineering a wide range of tissues, particularly for microscopic tissues that require proper controls of cell distribution and cell-cell organization [62]

5. Conclusions and Future Perspective of 4D Bioprinting

Even if the exciting developments brought by 4D bioprinting and predicting the possible changes that occur after process, intensive research and studies are needed to carry out. Especially in studies where living cells are used, changes in the biostructures during and after the bioprinting and their least effects should be precisely expected. Therefore, much more attention should be paid to the structural design of biostructures and biomaterials, and especially to other materials used such as crosslinkers. Combinational 3D and 4D studies can be used to interrogate and validate differential growth pattern and axonal tension patterns, as well as to evaluate the effects of mechanical stresses on neurodevelopment. In particular, the 4D bioprinter approach is an excellent methodology for studying the effects of cortical folding on stem cell proliferation and maturation, due to the ease of experimental manipulation and remarkable modifiability which provides. While the 4D bioprinter is still in its infancy as a fully fabrication technique, it may be rapidly adopted in the various tissue engineering disciplines include organ on a chip in the near coming years [66-70].

Acknowledgement

We gratefully acknowledge Turkish Scientific and Technological Council (TÜBİTAK) and Eskisehir Osmangazi University (Scientific Research Foundation) for their support.

References

1. Rothenbücher, T. S., Gürbüz, H., Pereira, M. P., Heiskanen, A., Emneus, J., & Martinez-Serrano, A. (2021). Next generation human brain models: engineered flat brain organoids featuring gyrification. Biofabrication, 13(1), 011001. doi: 10.1088/1758-5090/abc95e

2. Esworthy, T. J., Miao, S., Lee, S. J., Zhou, X., Cui, H., Zuo, Y. Y., & Zhang, L. G. (2019). Advanced 4D-bioprinting technologies for brain tissue modeling and study. International journal of smart and nano materials, 10(3), 177-204. doi: 10.1080/19475411.2019.1631899

3. Matsumoto, N., Shinmyo, Y., Ichikawa, Y., & Kawasaki, H. (2017). Gyrification of the cerebral cortex requires FGF signaling in the mammalian brain. Elife, 6, e29285 doi: 10.7554/eLife.29285

4. Nanda, P., Tandon, N., Mathew, I. T., Giakoumatos, C. I., Abhishekh, H. A., Clementz, B. A., Pearlson, G. D., Sweeney, J., Tamminga, C. A., & Keshavan, M. S. (2014). Local gyrification index in probands with psychotic disorders and their first-degree relatives. Biological psychiatry, 76(6), 447–455. doi: 10.1016/j.biopsych.2013.11.018

5. Thompson AJ, Pillai EK, Dimov IB, Foster SK, Holt CE, Franze K. Rapid changes in tissue mechanics regulate cell behaviour in the developing embryonic brain. Elife. 2019 Jan 15;8:e39356. doi: 10.7554/eLife.39356.

6. Askari, M., Naniz, M. A., Kouhi, M., Saberi, A., Zolfagharian, A., & Bodaghi, M. (2021). Recent progress in extrusion 3D bioprinting of hydrogel biomaterials for tissue regeneration: A comprehensive review with focus on advanced fabrication techniques. Biomaterials science, 9(3), 535-573. doi: 10.1039/D0BM00973C

7. Gao, W., Zhang, Y., Ramanujan, D., Ramani, K., Chen, Y., Williams, C. B., ... & Zavattieri, P. D. (2015). The status, challenges, and future of additive manufacturing in engineering. Computer-Aided Design, 69, 65-89. doi: 10.1016/j.cad.2015.04.001.

8. Farahani, R. D., Dubé, M., & Therriault, D. (2016). Three□dimensional printing of multifunctional nanocomposites: manufacturing techniques and applications. Advanced materials, 28(28), 5794-5821. doi: 10.1002/adma.201506215

9. Lee Ventola, C. (2014). Medical applications for 3D printing: current and projected uses, P T 39 (2014) 704–711

10. Guvendiren, M., Molde, J., Soares, R. M., & Kohn, J. (2016). Designing biomaterials for 3D printing. ACS biomaterials science & engineering, 2(10), 1679-1693. doi: 10.1021/acsbiomaterials.6b00121.

11. Kahl, M., Gertig, M., Hoyer, P., Friedrich, O., & Gilbert, D. F. (2019). Ultra-low-cost 3D bioprinting: modification and application of an off-the-shelf desktop 3D-printer for biofabrication. Frontiers in bioengineering and biotechnology, 7, 184. doi: 10.3389/fbioe.2019.00184.

12. Gao, B., Yang, Q., Zhao, X., Jin, G., Ma, Y., & Xu, F. (2016). 4D bioprinting for biomedical applications. Trends in biotechnology, 34(9), 746-756. doi: 10.1016/j.tibtech.2016.03.004

13. Mota, C., Camarero-Espinosa, S., Baker, M. B., Wieringa, P., & Moroni, L. (2020). Bioprinting: from tissue and organ development to in vitro models. Chemical reviews, 120(19), 10547-10607. doi: 10.1021/acs.chemrev.9b00789.

14. Cui, H., Nowicki, M., Fisher, J. P., & Zhang, L. G. (2017). 3D bioprinting for organ regeneration. Advanced healthcare materials, 6(1), 1601118. doi: 10.1002/adhm.201601118.

15. Xie, Z., Gao, M., Lobo, A. O., & Webster, T. J. (2020). 3D bioprinting in tissue engineering for medical applications: the classic and the hybrid. Polymers, 12(8), 1717. doi: 10.3390/POLYM12081717.

16. Wan, Z., Zhang, P., Liu, Y., Lv, L., & Zhou, Y. (2020). Four-dimensional bioprinting: Current developments and applications in bone tissue engineering. Acta biomaterialia, 101, 26-42. doi: 10.1016/j.actbio.2019.10.038.

17. Yu, C., Ma, X., Zhu, W., Wang, P., Miller, K. L., Stupin, J., ... & Chen, S. (2019). Scanningless and continuous 3D bioprinting of human tissues with decellularized extracellular matrix. Biomaterials, 194, 1-13. doi: 10.1016/j.biomaterials.2018.12.009.

18. Li, Y. C., Zhang, Y. S., Akpek, A., Shin, S. R., & Khademhosseini, A. (2016). 4D bioprinting: the next-generation technology for biofabrication enabled by stimuli-responsive materials. Biofabrication, 9(1), 012001. doi: 10.1088/1758-5090/9/1/012001.

19. Yang, G. H., Yeo, M., Koo, Y. W., & Kim, G. H. (2019). 4D bioprinting: technological advances in biofabrication. Macromolecular bioscience, 19(5), 1800441. doi: 10.1002/mabi.201800441.

20. Zhang, Z., Demir, K. G., & Gu, G. X. (2019). Developments in 4D-printing: a review on current smart materials, technologies, and applications. International Journal of Smart and Nano Materials, 10(3), 205-224. doi: 10.1080/19475411.2019.1591541.

21. Chadwick, M., Yang, C., Liu, L., Gamboa, C. M., Jara, K., Lee, H., & Sabaawy, H. E. (2020). Rapid processing and drug evaluation in glioblastoma patient-derived organoid models with 4D bioprinted arrays. Iscience, 23(8), 101365. doi: 10.1016/j.isci.2020.101365.

22. Amukarimi, S., & Mozafari, M. (2021). 4D bioprinting of tissues and organs. Bioprinting, e00161. doi: 10.1016/j.bprint.2021.e00161

23. Nadgorny, M., & Ameli, A. (2018). Functional polymers and nanocomposites for 3D printing of smart structures and devices. ACS applied materials & interfaces, 10(21), 17489-17507. doi: 10.1021/acsami.8b01786

24. Yang, Q., Gao, B., & Xu, F. (2020). Recent advances in 4D bioprinting. Biotechnology journal, 15(1), 1900086. doi: 10.1002/biot.201900086

25. Klouda, L., & Mikos, A. G. (2008). Thermoresponsive hydrogels in biomedical applications. European journal of pharmaceutics and biopharmaceutics, 68(1), 34-45. doi: 10.1016/j.ejpb.2007.02.025

26. Wang, X., Sun, Y., Peng, C., Luo, H., Wang, R., & Zhang, D. (2015). Transitional suspensions containing thermosensitive dispersant for three-dimensional printing. ACS applied materials & interfaces, 7(47), 26131-26136. doi: 10.1021/acsami.5b07913

27. Zarek, M., Mansour, N., Shapira, S., & Cohn, D. (2017). 4D printing of shape memory□based personalized endoluminal medical devices. Macromolecular rapid communications, 38(2), 1600628. doi: 10.1002/marc.201600628

28. Stoychev, G., Puretskiy, N., & Ionov, L. (2011). Self-folding all-polymer thermoresponsive microcapsules. Soft Matter, 7(7), 3277-3279. doi: 10.1039/C1SM05109A

29. Apsite, I., Stoychev, G., Zhang, W., Jehnichen, D., Xie, J., & Ionov, L. (2017). Porous stimuli-responsive self-folding electrospun mats for 4D biofabrication. Biomacromolecules, 18(10), 3178-3184.

30. Fratzl, P., & Barth, F. G. (2009). Biomaterial systems for mechanosensing and actuation. Nature, 462(7272), 442-448.

31. Lui, Y. S., Sow, W. T., Tan, L. P., Wu, Y., Lai, Y., & Li, H. (2019). 4D printing and stimuli-responsive materials in biomedical aspects. Acta biomaterialia, 92, 19-36. doi: 10.1016/j.actbio.2019.05.005

32. Gupta, M. K., Meng, F., Johnson, B. N., Kong, Y. L., Tian, L., Yeh, Y. W., ... & McAlpine, M. C. (2015). 3D printed programmable release capsules. Nano letters, 15(8), 5321-5329. doi: 10.1021/acs.nanolett.5b01688

33. Ahadian, S., Obregón, R., Ramón-Azcón, J., Salazar, G., Shiku, H., Ramalingam, M., & Matsue, T. (2016). Carbon nanotubes and graphene-based nanomaterials for stem cell differentiation and tissue regeneration. Journal of Nanoscience and Nanotechnology, 16(9), 8862-8880. doi: 10.1166/jnn.2016.12729

34. Ramon-Azcon, J., Ahadian, S., Obregon, R., Shiku, H., Ramalingam, M., & Matsue, T. (2014). Applications of carbon nanotubes in stem cell research. Journal of biomedical nanotechnology, 10(10), 2539-2561. doi: 10.1166/jbn.2014.1899

35. Sayyar, S., Bjorninen, M., Haimi, S., Miettinen, S., Gilmore, K., Grijpma, D., & Wallace, G. (2016). UV cross-linkable graphene/poly (trimethylene carbonate) composites for 3D printing of electrically conductive scaffolds. ACS applied materials & interfaces, 8(46), 31916-31925. doi: 10.1021/acsami.6b09962

36. Jakus, A. E., Secor, E. B., Rutz, A. L., Jordan, S. W., Hersam, M. C., & Shah, R. N. (2015). Three-dimensional printing of high-content graphene scaffolds for electronic and biomedical applications. ACS nano, 9(4), 4636-4648. doi: 10.1021/acsnano.5b01179

37. Kocak, G., Tuncer, C. A. N. S. E. L., & Bütün, V. J. P. C. (2017). pH-Responsive polymers. Polymer Chemistry, 8(1), 144-176. doi: 10.1039/C6PY01872F

38. Pourjavadi, A., Ebrahimi, A. A., & Barzegar, S. (2013). Preparation and evaluation of bioactive and compatible starch based superabsorbent for oral drug delivery systems. Journal of Drug Delivery Science and Technology, 23(5), 511-517. doi: 10.1016/S1773-2247(13)50074-8

39. Kwon, S. S., Kong, B. J., & Park, S. N. (2015). Physicochemical properties of pH-sensitive hydrogels based on hydroxyethyl cellulose–hyaluronic acid and for applications as transdermal delivery systems for skin lesions. European journal of pharmaceutics and biopharmaceutics, 92, 146-154. doi: 10.1016/j.ejpb.2015.02.025

40. Fundueanu, G., Constantin, M., Asmarandei, I., Harabagiu, V., Ascenzi, P., & Simionescu, B. C. (2013). The thermosensitivity of pH/thermoresponsive microspheres activated by the electrostatic interaction of pH□sensitive units with a bioactive compound. Journal of Biomedical Materials Research Part A, 101(6), 1661-1669. doi: 10.1002/jbm.a.34469

41. Kim, S. H., Seo, Y. B., Yeon, Y. K., Lee, Y. J., Park, H. S., Sultan, M. T., ... & Park, C. H. (2020). 4D-bioprinted silk hydrogels for tissue engineering. Biomaterials, 260, 120281. doi: 10.1016/j.biomaterials.2020.120281

42. Ramos, M. L. P., González, J. A., Fabian, L., Pérez, C. J., Villanueva, M. E., & Copello, G. J. (2017). Sustainable and smart keratin hydrogel with pH-sensitive swelling and enhanced mechanical properties. Materials Science and Engineering: C, 78, 619-626. doi: 10.1016/j.msec.2017.04.120

43. Narupai, B., Smith, P. T., & Nelson, A. (2021). 4D Printing of Multi□Stimuli Responsive Protein□Based Hydrogels for Autonomous Shape Transformations. Advanced Functional Materials, 2011012. doi: 10.1002/adfm.202011012

44. Yoshida, T., Lai, T. C., Kwon, G. S., & Sako, K. (2013). pH-and ion-sensitive polymers for drug delivery. Expert opinion on drug delivery, 10(11), 1497-1513. doi: 10.1517/17425247.2013.821978

45. Dong, Y., Wang, S., Ke, Y., Ding, L., Zeng, X., Magdassi, S., & Long, Y. (2020). 4D printed hydrogels: fabrication, materials, and applications. Advanced Materials Technologies, 5(6), 2000034. doi: 10.1002/admt.202000034

46. Rudko, M., Urbaniak, T., & Musiał, W. (2021). Recent Developments in Ion-Sensitive Systems for Pharmaceutical Applications. Polymers, 13(10), 1641. doi: 10.3390/polym13101641

47. Wang, B., Liu, L., & Liao, L. (2019). Light and ferric ion responsive fluorochromic hydrogels with high strength and self-healing ability. Polymer Chemistry, 10(47), 6481-6488. doi: 10.1039/C9PY01459D

48. Wu, Q., Wang, L., Yu, H., Wang, J., & Chen, Z. (2011). Organization of glucose-responsive systems and their properties. Chemical reviews, 111(12), 7855-7875. doi: 10.1021/cr200027j

49. Adams, A., Malkoc, A., & La Belle, J. T. (2018). The development of a glucose dehydrogenase 3D-printed glucose sensor: a proof-of-concept study. Journal of diabetes science and technology, 12(1), 176-182. doi: 10.1177/1932296817715272

50. Matsumoto, A., Ishii, T., Nishida, J., Matsumoto, H., Kataoka, K., & Miyahara, Y. (2012). A synthetic approach toward a self□regulated insulin delivery system. Angewandte Chemie International Edition, 51(9), 2124-2128. doi: 10.1002/anie.201106252

51. Brownlee, M., & Cerami, A. (1979). A glucose-controlled insulin-delivery system: semisynthetic insulin bound to lectin. Science, 206(4423), 1190-1191. doi: 10.1126/science.505005

52. Wang, J., Zhang, H., Wang, F., Ai, X., Huang, D., Liu, G., & Mi, P. (2018). Enzyme-responsive polymers for drug delivery and molecular imaging. In Stimuli Responsive Polymeric Nanocarriers for Drug Delivery Applications, Volume 1 (pp. 101-119). Woodhead Publishing. doi: 10.1016/B978-0-08-101997-9.00004-7

53. Zelzer, M., Todd, S. J., Hirst, A. R., McDonald, T. O., & Ulijn, R. V. (2013). Enzyme responsive materials: design strategies and future developments. Biomaterials Science, 1(1), 11-39. doi: 10.1039/C2BM00041E

54. Wang, X., Qin, X. H., Hu, C., Terzopoulou, A., Chen, X. Z., Huang, T. Y., ... & Nelson, B. J. (2018). 3D printed enzymatically biodegradable soft helical microswimmers. Advanced Functional Materials, 28(45), 1804107. doi: 10.1002/adfm.201804107

55. Banerjee, A., Arha, M., Choudhary, S., Ashton, R. S., Bhatia, S. R., Schaffer, D. V., Kane, R. S. (2009). The influence of hydrogel modulus on the proliferation and differentiation of encapsulated neural stem cells. Biomaterials. Sep;30(27):4695-9. doi: 10.1016/j.biomaterials.2009.05.050. Epub 2009 Jun 17.

56. Chang, Y. J., Tsai, C. J., Tseng, F. G., Chen, T. J., Wang, T. W. (2013). Micropatterned stretching system for the investigation of mechanical tension on neural stem cells behavior. Nanomedicine. Apr;9(3):345-55. doi: 10.1016/j.nano.2012.07.008. Epub 2012 Aug 24.

57. Lozano, R., Stevens, L., Thompson, B. C., Gilmore, K. J., Gorkin III, R., Stewart, E. M., in het Panhuis, M., Romero-Ortega, M. and Wallace, G.G. (2015). 3D printing of layered brain-like structures using peptide modified gellan gum substrates. Biomaterials, 67, 264-273. doi:10.1016/j.biomaterials.2015.07.022

58. Lorber, B., Hsiao, W. K., Hutchings, I. M., & Martin, K. R. (2013). Adult rat retinal ganglion cells and glia can be printed by piezoelectric inkjet printing. Biofabrication, 6(1), 015001. doi:10.1088/1758-5082/6/1/015001

59. Miao, S., Castro, N., Nowicki, M., Xia, L., Cui, H., Zhou, X., Zhu, W., Lee, S. J., Sarkar, K., Vozzi, G., Tabata, Y., Fisher, J., & Zhang, L. G. (2017). 4D printing of polymeric materials for tissue and organ regeneration. Materials today (Kidlington, England), 20(10), 577–591. doi: 10.1016/j.mattod.2017.06.005

60. Miao, S., Cui, H., Nowicki, M., Lee, S.J., Almeida, J., Zhou, X., Zhu, W., Yao, X., Masood, F., Plesniak, M.W. and Mohiuddin, M., 2018. Photolithographic-stereolithographic-tandem fabrication of 4D smart scaffolds for improved stem cell cardiomyogenic differentiation. Biofabrication, 10(3), p.035007. https://doi.org/10.1088/1758-5090/aabe0b

61. Miao, S., Cui, H., Nowicki, M., Xia, L., Zhou, X., Lee, S. J., ... & Zhang, L. G. (2018). Stereolithographic 4D bioprinting of multiresponsive architectures for neural engineering. Advanced biosystems, 2(9), 1800101. https://doi.org/10.1002/adbi.201800101

62. Cui, C., Kim, D. O., Pack, M. Y., Han, B., Han, L., Sun, Y., & Han, L. H. (2020). 4D printing of self-folding and cell-encapsulating 3D microstructures as scaffolds for tissue-engineering applications. Biofabrication, 12(4), 045018.

63. Zhu, W., George, J. K., Sorger, V. J., & Grace Zhang, L. (2017). 3D printing scaffold coupled with low level light therapy for neural tissue regeneration. Biofabrication, 9(2), 025002. doi:10.1088/1758-5090/aa6999

64. Melissinaki, V., Gill, A. A., Ortega, I., Vamvakaki, M., Ranella, A., Haycock, J. W., ... Claeyssens, F. (2011). Direct laser writing of 3D scaffolds for neural tissue engineering applications. Biofabrication, 3(4), 045005. doi:10.1088/1758-5082/3/4/045005

65. Raviv, D., Zhao, W., McKnelly, C., Papadopoulou, A., Kadambi, A., Shi, B., ... & Tibbits, S. (2014). Active printed materials for complex self-evolving deformations. Scientific reports, 4(1), 1-8. doi: 10.1038/srep07422

66. Zhang, Y. S., Aleman, J., Shin, S. R., Kilic, T., Kim, D., Shaegh, S. A. M., ... & Khademhosseini, A. (2017). Multisensor-integrated organs-on-chips platform for automated and continual in situ monitoring of organoid behaviors. Proceedings of the National Academy of Sciences, 114(12), E2293-E2302. doi: 10.1073/pnas.1612906114

67. Shin, S. R., Zhang, Y. S., Kim, D. J., Manbohi, A., Avci, H., Silvestri, A., ... & Khademhosseini, A. (2016). Aptamer-based microfluidic electrochemical biosensor for monitoring cell-secreted trace cardiac biomarkers. Analytical chemistry, 88(20), 10019-10027. doi: 10.1021/acs.analchem.6b02028

68. Shin, S. R., Kilic, T., Zhang, Y. S., Avci, H., Hu, N., Kim, D., ... & Khademhosseini, A. (2017). Label□Free and Regenerative Electrochemical Microfluidic Biosensors for Continual Monitoring of Cell Secretomes. Advanced Science, 4(5), 1600522. doi: 10.1002/advs.201600522

69. Hüseyin, A. V. C. I., GÜZEL, F. D., Salim, E. R. O. L., & Akpek, A. (2017). Recent advances in organ-on-a-chip technologies and future challenges: a review. Turkish Journal of Chemistry, 42(3), 587-610. doi:10.3906/kim-1611-35

70. Akpek, A., Öztürk, A. B., Alarçin, E., Huseyin, A. V. C. İ., & ADALI, M. A. Recent Advances in 4D Bioprinting. Research Journal of Biomedical and Biotechnology, 1(1), 20-23.

Review

THE SMALLEST WORKERS IN REGENERATIVE MEDICINE: STEM CELL-DERIVED EXOSOMES

Ozer Oner[1,2,3], Suleyman Gokhan Kara[1,2,4], Ihsan Burak Karakaya[1,2], Ayla Eker Sariboyaci [1,2], Onur Uysal [1,2], Sibel Gunes [1,2,] Huseyin Avci[1,2,5,6]

[1]Cellular Therapy and Stem Cell Production Application and Research Centre, ESTEM, Eskisehir Osmangazi University, Eskisehir, Turkey

[2]Department of Stem Cell, Institute of Health Sciences, Eskisehir Osmangazi University, Eskisehir, Turkey

[3]Suhut Vocational School of Health Services, Afyonkarahisar Health Sciences University, Afyonkarahisar, Turkey

[4]Department of Emergency Medicine, Eskisehir City Hospital, Eskisehir, Turkey

[5]Department of Metallurgical and Materials Engineering, Eskişehir Osmangazi University Eskişehir, Turkey

[6]Translational Medicine Research and Clinical Center, Eskisehir Osmangazi University, Eskisehir, Turkey

Abstract:

Extracellular vesicles (EVs) are secreted by cells into the extracellular space, which first discovered in 1967 as platelet dust. In recent years, the analysis of EVs treatment for various diseases has emerged in the studies to understand these vesicles' origin and biological functions. According to their size, biogenesis, content, release pathways and function, EVs have three main subtypes: microvesicle (MV), exosome (EX) and apoptotic body. EVs are found in all body fluids, including urine, plasma, and physiological fluids such as bronchial lavage. In addition, it is secreted by many cell types such as dendritic cells, B cells, T-cells, mast cells, tumour cells, and sperm. This review investigates the studies using stem cell-derived EVs in numerous clinical and preclinical research.

Keywords: Extracellular Vesicles, Stem Cell, Exosome, Regeneration, Regenerative Medicine.

Özet:

Ekstraselüler veziküller (EV), ilk olarak 1967'de trombosit tozu olarak keşfedilen, hücreler tarafından hücre dışı boşluğa salgılanan lipide bağlı veziküllerdir. Son yıllarda bu veziküllerin kökeninin ve biyolojik işlevlerinin anlaşılması için yapılan araştırmalarda EV'lerin çeşitli hastalıkların tedavilerinde kullanılabileceği fikri ortaya çıkmıştır. EV'lerin biyogenezlerine, salınım yollarına, boyutlarına, içeriğine ve işlevlerine göre farklılaşan, mikroveziküller (MV'ler), eksozomlar (EX) ve apoptotik cisimler olmak üzere üç ana alt tipi vardır. EV'ler; idrar, plazma ve bronşiyal lavaj gibi fizyolojik sıvılar dahil tüm vücut sıvılarında bulunurlar. Bunun yanında, B hücreleri, dendritik hücreler, mast hücreleri, T-hücreleri, tümör hücreleri, sperm gibi pek çok hücre tipi tarafından da salgılandığı gösterilmiştir. Bu derlemede çok sayıda klinik ve preklinik çalışmada kullanılan kök hücre kaynaklı EV'lerin terapötik etkinliğini gösteren çalışmaları derledik.

Anahtar Kelimeler: Ekstrasellüler veziküller, Kök Hücre, Eksozom, Rejenerasyon, Rejeneratif Tıp.

Correspondence Address : Ozer Oner Cellular Therapy and Stem Cell Production Application and Research Centre, ESTEM, Eskisehir Osmangazi University, Eskisehir, Turkey ozeroner@yandex.com

ORCID ID of the authors: O.O. 0000-0001-5352-7437, S.G. 0000-0002-7152-5643, İ.B.K. 0000-0001-7634-0771, A.E.S. 0000-0003-4536-9859, O.U. 0000-0001-6800-5607, S.G. 0000-0003-0846-1170, H.A. 0000-0002-2475-1963

Please cite this article in press at: Oner O., Kara S.G., Karakaya I.B., Sariboyaci A.E., Uysal O., Gunes S., Hüseyin Avcı H., The Smallest Workers in Regenerative Medicine: Stem Cell-Derived Exosomes, Journal of Medical Innovation and Technology, 2021; 3 (2):58-67 doi: 10.51934/jomit.1016923

1.Introduction

Besides the hormones and neurotransmitters released from the secretory vesicles of specialized cells, all the cells can secrete various membrane vesicles known as the extracellular vesicle (EV). This process has been preserved in evolutionary processes from bacteria to humans (1).

According to their size, release pathways, biogenesis, and function, EVs have three main subtypes: microvesicle (MV), exosome (EX) and apoptotic body. MVs are large vesicles formed by membrane budding, apoptotic bodies occur by bubbling into senescent or dying cells, and EXs are the smallest vesicles released from cells by the multivesicular endosomal route. EXs are, in general, 40-100 nm in diameter, contain 1.13-1.19 g/ml sucrose, and sedimenting at 100,000xg. Its membranes are rich in cholesterol, ceramide, sphingomyelin and lipid. EXs contain protein and RNA. Most EXs have protein sets such as tetraspanins (CD81, CD63 and CD9), TSG101 and Alix, and also contain tissue/cell type-specific proteins that indicate their cellular origin. Removal of unwanted proteins, protein-protein interaction, and intercellular communication in line with the exchange of proteins and genetic materials are among the critical functions of EXs. EXs also play an essential role in the transfer of proteomic and genomic materials between the cells.

EVs carry components of the cells from which they are produced. In animal models and clinical studies, it has been reported that tissue and cellular functions show similar regenerative effects with the cells from which they are produced. The molecular mechanisms of the contents, secretion, uptake and function of EXs form the basis of preclinical studies. This intercellular communication of EVs has brought the view that the desired therapeutic molecule can be loaded and used as a natural drug deliverer (Table 1) (2–4). Stem cells can transform into different cell types, replace injured tissues, and repair at the injury site with a paracrine mechanism of action. Stem cell in vivo studies has been used successfully to treat graft-versus-host disease (GvHD), haematological malignancies, autoimmune diseases, and acute thrombocytopenia (5–7).

Table 1. Properties of exosomes [2].

Size (nm)	40-100
Biogenesis	Exocytosis of multivesicular bodies
Markers	CD63, CD81, CD9, Tsg101, Alix, Hsc70.
Contents	Proteins, lipids, mRNA and microRNA and rarely DNA.

Whether EXs will be superior to angiogenic drugs, recombinant growth factors, other peptides, and stem cell-based therapies is unclear and is a crucial issue to be investigated. As a result of in vitro and in vivo characterization analyses performed till now, EXs are emerging as a popular cell-free candidate that can be used to overcome many of the challenges posed by using cells as therapeutic agents. It has been used as a source of cell-free therapy in animal models of many tissues damage and diseases (8,9).

2. Mechanism of Action and Biologıcal Effects of Exosomes

The genetic material of EXs and MVs is transferred locally and systematically. EV-mediated therapeutic effects are thought to be due to two different mechanisms: First; EVs released from damaged tissues can act on local stem cells and regulate the release of regenerative microvesicles for tissue repair (10). Latter; local stem cells around damaged or degenerated tissues can produce microvesicles to stimulate regeneration, re-enter the cell cycle near damaged tissues and enable dedifferentiation.

Investigating the relationship between wound repair and SC-EV in preclinical studies contributes to paving the way for SC-EVs in clinical studies (11–13). Preclinical studies have demonstrated that SC-EVs may repair tissue damage by maintaining stemness, induction of regeneration, inhibition of apoptosis, and immunoregulation (Table 2).

SC-EVs can protect against cell apoptosis and reduce tissue damage. Human umbilical cord-derived mesenchymal stem cell extracellular vesicles (hUC-MSC-EVs) can carry antioxidant enzymes, and manganese superoxide dismutase in mitochondria inhibit oxidative stress-induced hepatocyte apoptosis and protect against hepatic Ischaemia-Reperfusion injury (IRI) in rats (14–17).

3. Stem Cell Culture for Extracellular Vesicle Production

3.1. Stem Cell Selection

The secretion of EVs is also affected by the senescence of MSCs (18–21). Abello et al. (2019), hUC-MSC-EXs gadolinium lipid (GdL-EXs) or infrared dye in tumour-bearing mice, 1,1'-dioctadecyl-3,3,3',3'-tetramethylindotricarbocyanine iodide (DiR-EXs), analyzed the biodistribution of EXs by labelling them (22). Intravenous infusion of lower doses of EV showed relatively higher hepatic accumulation compared to higher doses (22,23) (Fig. 1).

Table 2. Experimental model diseases treated with different stem cell-derived EVs.

Indication	Species	EV Sources	Main outcome	Mechanism	Reference
Traumatic brain injury (TBI)	Rat	Human AdMSC-EXs	Improvement of motor behavior function and cortical brain injury	Delivering MALAT1	[24]
Stroke	Rat	Rat BMSC-EXs	Neurite remodeling	Neurogenesis	[25]
Alzheimer's disease	Mouse	EXs from hypoxia-stimulated BMSCs	Learning and memory abilities	Restoration of synaptic dysfunction and regulation of inflammatory responses through miR-21	[26]
Spinal cord injury (SCI)	Rat	BMSC-EXs	Improvement of functional behavioral recovery effects	Activation of A1 neurotoxic reactive astrocytes	[27]
Spinal cord injury	Rat	Human BMSC-EVs	Inflammatory response, improved motor function, enhanced mechanical sensitivity threshold	uncertain	[28]
Spinal cord injury	Mouse	hucMSC-EXs	Improving functional recovery	Decreases inflammation	[29]
Myocardial infarction	Mouse	iPSC-EVs	Preservation of viable myocardium	Delivery of ESC specific miR-294	[30]
Myocardial infarction	Mouse	Mouse ESC-EXs	Resurgence of cardiac proliferative response	Delivering miR-294	[31]
Myocardial infarction	Mouse	Mouse BMSC-EVs	Improving cardiac function	Delivering miR-210	[32]
Myocardial infarction	Mouse	EXs derived from hypoxia-stimulated BMSC	Better cardiac functions recovery	Delivering miR-210	[33]
Lung injury	Mouse	Human BMSC-EVs	Reduces pulmonary vascular permeability	Modulating cytoskeletal signaling	[34]
Acute lung injury	Mouse	Human BMSC-MVs	Reduces pulmonary capillary permeability	Delivering Angiopoietin-1 mRNA and immune regulation	[35]
Neonatal hyperoxic lung injury	Rat	hUCB-MSC-EVs	Reduces impaired alveolarization and angiogenesis	Transfer of VEGF protein	[36]
Liver injury	Mouse	Mouse BMSC-EVs	Increase the mRNA expression of anti-inflammatory cytokines	Immunosuppression and immune protection	[37]

Renal ischemia/reperfusion injury	Rat	hiPSC-MSC-EVs	Decrease serum levels of creatinine and urea nitrogen	Exosomal SP1 activating the expression of SK1 and the generation of S1P	[42]
Rejuvenation of skin	Human skin tissues	hUCB-MSC-EXs	Increase expressions of Collagen I and Elastin	Uncertain	[44]
Wound healing	Mouse	hucMSC-EXs	Decrease scar formation and myofibroblast accumulation	Transfer of specific microRNAs and suppression of TGF-β /Smad2 pathway	[45]
Osteoporosis	Rat	hiPSC-MSC-EXs	Preventing bone loss	Activation of the PI3K/Akt signaling pathway	[41]
Stabilized fracture	Rat	hucMSC-EXs	Increase angiogenesis and bone healing	HIF-1alpha mediated promotion of angiogenesis	[47]
Osteogenesis imperfecta	Mouse	Murine BMSC-EVs	Facilitating bone growth	Delivery of miRNAs	[48]

4. Use of Stem Cell-Derived Exosomes in Treatment

4.1. Exosomes in Neurological Diseases

In recent years, it has been reported that EXs are effective in the pathogenesis of neural diseases. E.g., EXs are released from neurons, astrocytes and glial cells to facilitate different functions such as removing unwanted stress proteins and amyloid fibril formation. EXs containing α-synuclein have been shown to induce cell death in neuronal cells, suggesting that EXs potentiate and increase Parkinson's disease pathology. Again, in Alzheimer's disease, β-amyloid is released in association with EXs (24).

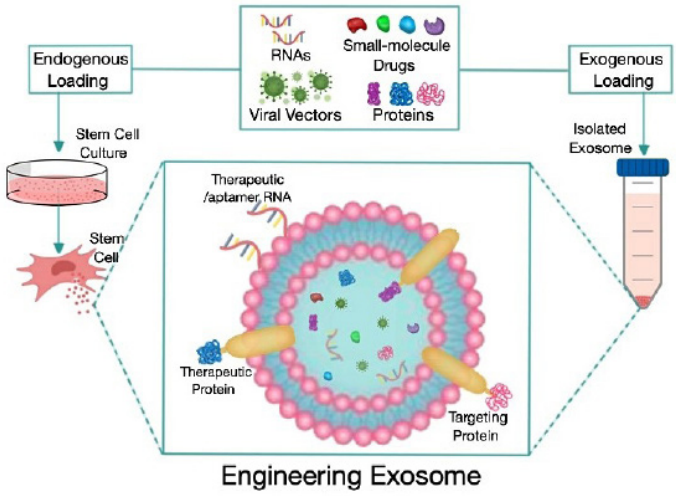

Figure 1. Engineering EVs. Extracellular vesicles (EVs) can provide therapeutic assets, including proteins, RNAs, oncolytic viruses, and small molecule drugs by endogenous loading during EV biogenesis or by exogenous loading after EV isolation. Engineered EVs can express targeted peptides or therapeutic proteins on their surface and bind aptamers or therapeutic RNAs via RNA-binding proteins.

In animal models of brain injury, systemic administration of SC-EXs has been shown to reduce neuroinflammation. (25–27). Traumatic spinal cord injuries can cause clinical conditions up to complete loss of motor and sensation in the lower extremities (28,29). Sun et al. (2018), in a study on rats, showed that UC-MSC-EXs support functional recovery in spinal cord injuries by reducing inflammation (30). Liu et al. (2021) reported that MSC-EVs pretreated with melatonin recovered the traumatic spinal cord injury with NRF2 stabilization (19).

4.2. Exosomes in Cardiovascular Diseases

The proliferation abilities of cardiomyocytes usually are pretty poor (31–33). Sun et al. (2018), in a study, conducted, in an animal model of dilated cardiomyopathy induced by doxorubicin: They have resulted that BM-MSC-EXs improved cardiac function, inhibited cardiac dilation, attenuated cardiomyocyte apoptosis, decreased the number of pro-inflammatory macrophages in the infiltration zone and the expression of inflammatory factors (34).

4.3. Exosomes in Lung Diseases

Potter et al. (2018) showed that BM-MSC-EVs could significantly reduce pulmonary vascular permeability induced by hemorrhagic shock in mice through regulation of cytoskeletal signalling (35). In another study, Tang et al. (2017) showed that BM-MSC-MVs, administering angiopoietin-1 (Ang-1) mRNAs to mice, can support the stability of the pulmonary vasculature and reduce inflammation in the lungs (36).

On the other hand, Sengupta et al. (2020) conducted a phase I clinical study showing that BM-MSC-EXs can be used safely in lung damage due to COVID-19 (37). With the increase in clinical studies, it is predicted that SC-EXs will enter our daily routine in respiratory system diseases.

4.4. Exosomes in Gastrointestinal Diseases

4.4.1. Intestines

Inflammatory bowel diseases (IBD) are considered chronic, recurrent inflammatory diseases that can affect any part of the gastrointestinal tract. IBD includes two diseases, Crohn's disease and ulcerative colitis. Although both diseases usually have similar clinical manifestations, they affect different parts of the gastrointestinal tract, and the degree of intestinal wall inflammation may differ (38).

There is evidence that EXs play a role in the pathogenesis of IBD. Macrophage pyroptosis, a cell death process after inflammatory activation of NOD-like receptor family pyrin domain-containing 3 (NLRP3), is thought to be part of the cause of an abnormal immune response in IBD pathogenesis. Macrophage pyroptosis plays an essential regulatory role in reducing colitis by hUC-MSC-EXs. Cai et al. (2021), in their in vivo experiments, showed that hUC-MSC-EXs inhibited the activation of NLRP3 inflammations in the mouse colon and inhibited the secretion of IL-1β, IL-18 and Caspase-1 cleavage, resulting in a decrease in cell pyroptosis (39). Barnhoorn et al. (2020) demonstrated that local application of BM-MSC-EX as a cell-free substitute for MSC therapy in an animal model of IBD reduces intestinal epithelial damage by stimulating epithelial regeneration (40).

4.4.2. Liver

Studies have shown that SC-EVs can treat liver diseases by the administration of various active molecules. In animal models of liver injury, the use of SC-EXs has been found to reduce injury and increase regeneration (41–43). In addition, studies have revealed that hUC-MSC-EXs can alleviate liver fibrosis in mice by inactivating TGF-β/Smad signalling, reducing collagen deposition and inflammation (44). hUC-MSC-EXs carrying glutathione peroxidase-1 have been shown to protect against liver failure in mice by reducing inflammation and oxidative stress (45).

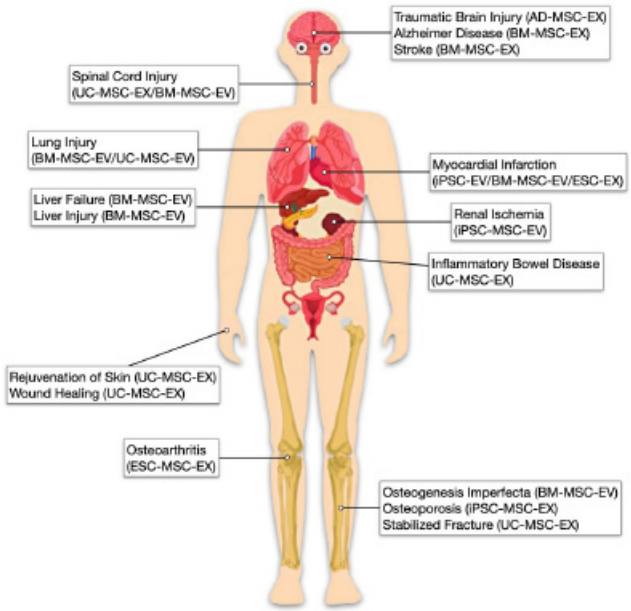

Figure 2. Schematic representation of diseases treatment with exosomes isolated from stem cells through different sources.

4.5. Exosomes in Ocular Disease

Preclinical studies have shown that the administration of MSC-EXs can protect against retinal ischemia (46). Shen et al. showed that AD-MSC-EX treatment regulates CSC proliferation, inhibits apoptosis, triggers higher collagen and fibronectin expression, and causes lower expression of matrix metalloproteinases in vitro (47).

4.6. Exosomes in Renal Diseases

Preclinical studies have shown that SC-EVs have a positive effect on kidney disease. EVs from human iPSC-derived MSCs (hiPSC-MSC-EVs) transport the specificity protein (SP1) to renal tubular epithelial cells, increasing the expression of sphingosine kinase 1 and inhibiting necroptosis, thus, showed that it prevents renal IRI in rats (48).

Tomasoni et al. (2013) revealed that BMSC-EXs transport insulin-like growth factor 1 (IGF-1) receptor mRNAs to renal tubular epithelial cells in vitro; these mRNAs are then translated into IGF-1 receptor proteins, which can be used to increase the sensitivity of the IGF-1 receptor to local IGF-1 and to treat cisplatin-induced renal tubule injury (49).

5. Conclusion and Future Perspectives

SC-EV therapy has made significant progress in regenerative medicine and numerous preclinical trials, laying a solid foundation for clinical transformation practice. It is important to note that selecting an early passage of EV-producing cells, optimizing techniques of cell culture conditions, and using EVs for delivery of genomic materials, proteins, or small-molecule drugs can increase their efficacy against many diseases.

However, we still have a long way to go before the clinical application of EVs. Current research mainly focuses on treating a limited number of diseases in regenerative medicine and oncology using SC-EVs. The functions of SC-EVs should be tested for many other diseases.

High-quality EVs are needed for successful results in studies. To obtain higher quality EVs, it is necessary to select the appropriate culture medium, optimize cell density, cell phenotype, culture time, collection time and other parameters. Furthermore, pre-condition EVs are similarly crucial.

On the other hand, the drug loading potential of SC-EVs should be further investigated. Genome editing techniques currently facilitate EV engineering with different contents and functions but can cause indeterminate mutations in EV-producing cells, affecting the contents and functions of related EVs. Therefore, it is necessary to improve the safety and operability of genome editing techniques, reduce off-target efficiency, and

ultimately accurately produce EVs with specific functions and components.

It is imperative to improve the drug loading efficiency of EV by novel methods. Exogenous drugs are currently loaded into EVs mainly by electroporation, but the efficacy of this technique is insufficient. Although drug loading efficacy is not proportional to therapeutic efficacy, balancing these two types of efficacies is recommended. Therefore, optimum drug concentrations with the lowest side effects may be preferred to achieve the highest therapeutic efficacy. For this, we still need to increase drug loading efficiency.

The advantages and excellent application potential of SC-EVs are driving the advancement of regenerative medicine. The future development goal should be to optimize EV production conditions, improve production technology, improve yield and quality, measure their therapeutic efficacy, design operations to give EVs more therapeutic functions, and ultimately drive their clinical transformation to benefit people more broadly. On the other hand, it is considered to have potential limitations. For example, EXs are a mixture of biologically active molecules. Some of these molecules may have beneficial effects under certain conditions, while others may have a detrimental effect (e.g., pro-inflammatory). Whether exosomes will be superior to angiogenic drugs or purified recombinant growth factors and other peptides in the context of cell-free approaches for tissue regeneration is unclear and remains an important issue to be explored.

References

1. Liu W, Ma Z, Li J, Kang X. Mesenchymal stem cell-derived exosomes: therapeutic opportunities and challenges for spinal cord injury. Stem Cell Research & Therapy. 2021 Dec 3;12(1).

2. Biancone L, Bruno S, Deregibus MC, Tetta C, Camussi G. Therapeutic potential of mesenchymal stem cell-derived microvesicles. Nephrology Dialysis Transplantation. 2012 Aug 1;27(8).

3. Lai RC, Yeo RWY, Tan KH, Lim SK. Exosomes for drug delivery — a novel application for the mesenchymal stem cell. Biotechnology Advances. 2013 Sep;31(5).

4. Gutierrez□Millan C, Calvo Díaz C, Lanao JM, Colino CI. Advances in Exosomes□Based Drug Delivery Systems. Macromolecular Bioscience. 2021 Jan 22;21(1).

5. Semedo P, Burgos-Silva M, Donizetti-Oliveira C, Saraiva Camar NO. How do Mesenchymal Stem Cells Repair? In: Stem Cells in Clinic and Research. InTech; 2011.

6. Güneş S, Uysal O, Sevimli T, Sevimli M, Tokhi A, Sarıboyacı A. Kök Hücreler. In: Avci H, editor. Polimerler: Özellikleri ve Uygulamaları. 1st ed. ESOGU; 2021. p. 325–49.

7. Song Y, Kim Y, Ha S, Sheller□Miller S, Yoo J, Choi C, et al. The emerging role of exosomes as novel therapeutics: Biology, technologies, clinical applications, and the next. American Journal of Reproductive Immunology. 2021 Feb 12;85(2).

8. E Z, G. M, Momen-Heravi F, Hu J, Zhang X, Wu Y, et al. Therapeutic uses of exosomes. Exosomes and Microvesicles. 2013

9. Watanabe Y, Tsuchiya A, Terai S. The development of mesenchymal stem cell therapy in the present, and the perspective of cell-free therapy in the future. Clinical and Molecular Hepatology. 2021 Oct;27(1)

10. Khan M, Nickoloff E, Abramova T, Johnson J, Verma SK, Krishnamurthy P, et al. Embryonic Stem Cell–Derived Exosomes Promote Endogenous Repair Mechanisms and Enhance Cardiac Function Following Myocardial Infarction. Circulation Research. 2015 Oct;117(1).

11. Ranghino A, Bruno S, Bussolati B, Moggio A, Dimuccio V, Tapparo M, et al. The effects of glomerular and tubular renal progenitors and derived extracellular vesicles on recovery from acute kidney injury. Stem Cell Research & Therapy. 2017 Oct;8(1).

12. McBride JD, Rodriguez-Menocal L, Guzman W, Candanedo A, Garcia-Contreras M, Badiavas E v. Bone Marrow Mesenchymal Stem Cell-Derived CD63 + Exosomes Transport Wnt3a Exteriorly and Enhance Dermal Fibroblast Proliferation, Migration, and Angiogenesis In Vitro. Stem Cells and Development. 2017 Oct;26(19).

13. Zhang S, Chuah SJ, Lai RC, Hui JHP, Lim SK, Toh WS. MSC exosomes mediate cartilage repair by enhancing proliferation, attenuating apoptosis and modulating immune reactivity. Biomaterials. 2018 Oct;156.

14. Yao J, Zheng J, Cai J, Zeng K, Zhou C, Zhang J, et al. Extracellular vesicles derived from human umbilical cord mesenchymal stem cells alleviate rat hepatic ischemia□ reperfusion injury by suppressing oxidative stress and neutrophil inflammatory response. The FASEB Journal. 2019 Oct;33(2).

15. Li X, Liu L, Yang J, Yu Y, Chai J, Wang L, et al. Exosome Derived From Human Umbilical Cord Mesenchymal Stem Cell Mediates MiR-181c Attenuating Burn-induced Excessive Inflammation. EBioMedicine. 2016 Oct;8.

16. Fujii S, Miura Y, Fujishiro A, Shindo T, Shimazu Y, Hirai H, et al. Graft-Versus-Host Disease Amelioration by Human Bone Marrow Mesenchymal Stromal/Stem Cell-Derived Extracellular Vesicles Is Associated with Peripheral Preservation of Naive T Cell Populations. STEM CELLS. 2018 Oct;36(3).

17. Fan Y, Herr F, Vernochet A, Mennesson B, Oberlin E, Durrbach A. Human Fetal Liver Mesenchymal Stem Cell-Derived Exosomes Impair Natural Killer Cell Function. Stem Cells and Development. 2019 Oct;28(1).

18. Kulkarni R, Bajaj M, Ghode S, Jalnapurkar S, Limaye L, Kale VP. Intercellular Transfer of Microvesicles from Young Mesenchymal Stromal Cells Rejuvenates Aged Murine Hematopoietic Stem Cells. STEM CELLS. 2018 Oct;36(3).

19. Liu W, Tang P, Wang J, Ye W, Ge X, Rong Y, et al. Extracellular vesicles derived from melatonin□preconditioned mesenchymal stem cells containing USP29 repair traumatic spinal cord injury by stabilizing NRF2. Journal of Pineal Research. 2021 Oct;

20. Wang X, Omar O, Vazirisani F, Thomsen P, Ekström K. Mesenchymal stem cell-derived exosomes have altered microRNA profiles and induce osteogenic differentiation depending on the stage of differentiation. PLOS ONE. 2018 Oct;13(2).

21. Cui G, Wu J, Mou F, Xie W, Wang F, Wang Q, et al. Exosomes derived from hypoxia□preconditioned mesenchymal stromal cells ameliorate cognitive decline by rescuing synaptic dysfunction and regulating inflammatory responses in APP/PS1 mice. The FASEB Journal. 2018 Oct;32(2).

22. Abello J, Nguyen TDT, Marasini R, Aryal S, Weiss ML. Biodistribution of gadolinium- and near infrared-labeled human umbilical cord mesenchymal stromal cell-derived exosomes in tumor bearing mice. Theranostics. 2019;9(8).

23. Wiklander OPB, Nordin JZ, O'Loughlin A, Gustafsson Y, Corso G, Mäger I, et al. Extracellular vesicle in vivo biodistribution is determined by cell source, route of administration and targeting. Journal of Extracellular Vesicles. 2015 Oct;4(1).

24. Patel NA, Moss LD, Lee J-Y, Tajiri N, Acosta S, Hudson C, et al. Long noncoding RNA MALAT1 in exosomes drives regenerative function and modulates inflammation-linked networks following traumatic brain injury. Journal of Neuroinflammation. 2018 Oct;15(1).

25. Kim D, Nishida H, An SY, Shetty AK, Bartosh TJ, Prockop DJ. Chromatographically isolated CD63 + CD81 + extracellular vesicles from mesenchymal stromal cells rescue cognitive impairments after TBI. Proceedings of the National Academy of Sciences. 2016 Oct;113(1).

26. Xin H, Katakowski M, Wang F, Qian J-Y, Liu XS, Ali MM, et al. MicroRNA-17–92 Cluster in Exosomes Enhance Neuroplasticity and Functional Recovery After Stroke in Rats. Stroke. 2017 Oct;48(3).

27. de Godoy MA, Saraiva LM, de Carvalho LRP, Vasconcelos-dos-Santos A, Beiral HJ v, Ramos AB, et al. Mesenchymal stem cells and cell-derived extracellular vesicles protect hippocampal neurons from oxidative stress and synapse damage induced by amyloid-β oligomers. Journal of Biological Chemistry. 2018 Oct;293(6).

28. Liu W, Wang Y, Gong F, Rong Y, Luo Y, Tang P, et al. Exosomes Derived from Bone Mesenchymal Stem Cells Repair Traumatic Spinal Cord Injury by Suppressing the Activation of A1 Neurotoxic Reactive Astrocytes. Journal of Neurotrauma. 2019 Oct;36(3).

29. Ruppert KA, Nguyen TT, Prabhakara KS, Furman NET, Srivastava AK, Harting MT, et al. Human Mesenchymal Stromal Cell-Derived Extracellular Vesicles Modify Microglial Response and Improve Clinical Outcomes in Experimental Spinal Cord Injury. Scientific Reports. 2018 Oct;8(1).

30. Sun G, Li G, Li D, Huang W, Zhang R, Zhang H, et al. hucMSC derived exosomes promote functional recovery in spinal cord injury mice via attenuating inflammation. Materials Science and Engineering: C. 2018 Aug;89.

31. Adamiak M, Cheng G, Bobis-Wozowicz S, Zhao L, Kedracka-Krok S, Samanta A, et al. Induced Pluripotent Stem Cell (iPSC)–Derived Extracellular Vesicles Are Safer and More Effective for Cardiac Repair Than iPSCs. Circulation Research. 2018 Oct;122(2).

32. Wang N, Chen C, Yang D, Liao Q, Luo H, Wang X, et al. Mesenchymal stem cells-derived extracellular vesicles, via miR-210, improve infarcted cardiac function by promotion of angiogenesis. Biochimica et Biophysica Acta (BBA) - Molecular Basis of Disease. 2017 Aug;1863(8).

33. Zhu J, Lu K, Zhang N, Zhao Y, Ma Q, Shen J, et al. Myocardial reparative functions of exosomes from mesenchymal stem cells are enhanced by hypoxia treatment of the cells via transferring microRNA-210 in an nSMase2-dependent way. Artificial Cells, Nanomedicine, and Biotechnology. 2017 Oct;

34. Sun X, Shan A, Wei Z, Xu B. Intravenous mesenchymal stem cell-derived exosomes ameliorate myocardial inflammation in the dilated cardiomyopathy. Biochemical and Biophysical Research Communications. 2018 Oct;503(4).

35. Potter DR, Miyazawa BY, Gibb SL, Deng X, Togaratti PP, Croze RH, et al. Mesenchymal stem cell-derived extracellular vesicles attenuate pulmonary vascular permeability and lung injury induced by hemorrhagic shock and trauma. Journal of Trauma and Acute Care Surgery. 2018 Oct;84(2).

36. Tang X-D, Shi L, Monsel A, Li X-Y, Zhu H-L, Zhu Y-G, et al. Mesenchymal Stem Cell Microvesicles Attenuate Acute Lung Injury in Mice Partly Mediated by Ang-1 mRNA. STEM CELLS. 2017 Jul;35(7).

37. Sengupta V, Sengupta S, Lazo A, Woods P, Nolan A, Bremer N. Exosomes Derived from Bone Marrow Mesenchymal Stem Cells as Treatment for Severe COVID-19. Stem Cells and Development. 2020 Oct;29(12).

38. Younis N, Zarif R, Mahfouz R. Inflammatory bowel disease: between genetics and microbiota. Molecular Biology Reports. 2020 Oct;47(4).

39. Cai X, Zhang Z, Yuan J, Ocansey DKW, Tu Q, Zhang X, et al. hucMSC-derived exosomes attenuate colitis by regulating macrophage pyroptosis via the miR-378a-5p/NLRP3 axis. Stem Cell Research & Therapy. 2021 Oct;12(1).

40. Barnhoorn MC, Plug L, Jonge ESMM, Molenkamp D, Bos E, Schoonderwoerd MJA, et al. Mesenchymal Stromal Cell–Derived Exosomes Contribute to Epithelial Regeneration in Experimental Inflammatory Bowel Disease. Cellular and Molecular Gastroenterology and Hepatology. 2020;9(4).

41. Haga H, Yan IK, Takahashi K, Matsuda A, Patel T. Extracellular Vesicles from Bone Marrow-Derived Mesenchymal Stem Cells Improve Survival from Lethal Hepatic Failure in Mice. STEM CELLS Translational Medicine. 2017 Oct;6(4).

42. Tamura R, Uemoto S, Tabata Y. Immunosuppressive effect of mesenchymal stem cell-derived exosomes on a concanavalin A-induced liver injury model. Inflammation and Regeneration. 2016 Oct;36(1).

43. Rigo F, Stefano N de, Navarro-Tableros V, David E, Rizza G, Catalano G, et al. Extracellular Vesicles from Human Liver Stem Cells Reduce Injury in an Ex Vivo Normothermic Hypoxic Rat Liver Perfusion Model. Transplantation. 2018 Oct;102(5).

44. Li T, Yan Y, Wang B, Qian H, Zhang X, Shen L, et al. Exosomes Derived from Human Umbilical Cord Mesenchymal Stem Cells Alleviate Liver Fibrosis. Stem Cells and Development. 2013 Oct;22(6).

45. Yan Y, Jiang W, Tan Y, Zou S, Zhang H, Mao F, et al. huc-MSC Exosome-Derived GPX1 Is Required for the Recovery of Hepatic Oxidant Injury. Molecular Therapy. 2017 Oct;25(2).

46. Moisseiev E, Anderson JD, Oltjen S, Goswami M, Zawadzki RJ, Nolta JA, et al. Protective Effect of Intravitreal Administration of Exosomes Derived from Mesenchymal Stem Cells on Retinal Ischemia. Current Eye Research. 2017 Oct;42(10).

47. Shen T, Zheng Q-Q, Shen J, Li Q-S, Song X-H, Luo H-B, et al. Effects of Adipose-derived Mesenchymal Stem Cell Exosomes on Corneal Stromal Fibroblast Viability and Extracellular Matrix Synthesis. Chinese Medical Journal. 2018 Oct;131(6).

48. Yuan X, Li D, Chen X, Han C, Xu L, Huang T, et al. Extracellular vesicles from human-induced pluripotent stem cell-derived mesenchymal stromal cells (hiPSC-MSCs) protect against renal ischemia/reperfusion injury via delivering specificity protein (SP1) and transcriptional activating of sphingosine kinase 1 and inhibiting necroptosis. Cell Death & Disease. 2017 Oct;8(12).

49. Tomasoni S, Longaretti L, Rota C, Morigi M, Conti S, Gotti E, et al. Transfer of Growth Factor Receptor mRNA Via Exosomes Unravels the Regenerative Effect of Mesenchymal Stem Cells. Stem Cells and Development. 2013 Oct;22(5).